Genetic analysis of RNA polymerase I unveils new role of the Rpa12 subunit during transcription

Tommy Darrière[1], Michael Pilsl[2], Adrien Chauvier[1], Titouan Genty[1], Sylvain Audibert[1], Christophe Dez[1], Isabelle Leger-Silvestre[1], Christophe Normand[1], Olga Calvo[3], Carlos Fernández-Tornero[4], Herbert Tschochner[2] and Olivier Gadal[1]

[1] Laboratoire de Biologie Moléculaire Eucaryote, Centre de Biologie Intégrative (CBI), Université de Toulouse, CNRS, UPS, 31000, Toulouse, France

[2]Universität Regensburg, Biochemie-Zentrum Regensburg (BZR), Lehrstuhl Biochemie III, 93053 Regensburg, Germany

[3]Instituto de Biología Funcional y Genómica, IBFG-CSIC, Universidad de Salamanca, Zacarías González 2, 37007 Salamanca, Spain

[4]Centro de Investigaciones Biológicas, CSIC, Ramiro de Maeztu 9, 28040 Madrid, Spain

Summary: (174 words)

Most transcriptional activity of exponentially growing cells is carried out by RNA Polymerase I (Pol I), which produces a large rRNA precursor. The Pol I transcription cycle is achieved through complex structural rearrangements of the enzyme, revealed by recent structural studies. In the yeast *S. cerevisiae* the Pol 1 subunit Rpa49, particularly its C-terminal tandem winged helix domain (Rpa49Ct), is required supports both initiation and elongation of the transcription cycle. Here, we characterized novel extragenic suppressors of the growth defect caused by the absence of Rpa49. We identified suppressor mutations on the two largest subunits of Pol I, Rpa190 and Rpa135, as well as Rpa12. Suppressor mutants *RPA135-F301S* and *RPA12-S6L* restored normal rRNA synthesis and increased Pol I density on rDNA genes in the absence of Rpa49Ct. Most mutated residues cluster at an interface formed by the jaw in Rpa190, the lobe in Rpa135, and subunit Rpa12 when mapped on the structure of Pol I. Our genetic data in *S. cerevisiae* suggest a new role for Rpa12 at the jaw/lobe interface during transcription cycle.

Introduction

The nuclear genome of eukaryotic cells is transcribed by three RNA polymerases (Chambon, 1975). RNA polymerase II (Pol II) transcribes most of the genome and is responsible for all messenger RNA production. RNA polymerases III and I are specialized in the synthesis of a limited number of transcripts. RNA polymerase III (Pol III) produces small structured RNAs, including tRNAs and the 5S ribosomal RNA. RNA polymerase I (Pol I) produces a single transcript, the large polycistronic precursor (the 35S pre-rRNA in yeast), processed by multiple successive steps into the mature rRNAs (25S, 18S, and 5.8S in yeast). Despite producing a single transcript, Pol I is by far the most active eukaryotic RNA polymerase, responsible for up to 60% of the total transcriptional activity in exponentially growing cells (Warner, 1999). Pol I rRNA synthesis constitutes the first step of ribosome biogenesis and is a rate limiting process for cell growth. The strongly transcribed rRNA genes can be visualized using the DNA spread method developed by Miller *et al*, 1969, in which the 35S rRNA genes (rDNA) adopt a "Christmas tree" conformation, with up to 120 polymerases per transcribed gene (Miller & Beatty, 1969). Altered cell proliferation, often associated with a modified rate of rRNA synthesis via the deregulation of Pol I activity, has been associated with various types of cancer (Drygin *et al*, 2010).

The full subunit composition and structural data are now available for the three nuclear RNA polymerases of the budding yeast *Saccharomyces cerevisiae* (Fernández-Tornero *et al*, 2013; Engel *et al*, 2013); (Hoffmann *et al*, 2015; Cramer *et al*, 2001). Pol I contains a core of shared or homologous subunits that are largely conserved in eukaryotes and archaea, as for the other two nuclear RNA polymerases (Werner, 2008). The two largest subunits (Rpa190 and Rpa135) carry the catalytic site. Rpb5, Rpb6, Rpb8, Rpb10, and Rpb12 are shared with Pol II and Pol III, whereas Rpc40 and Rpc19 are only shared with Pol III. This nine-subunit core is associated with the stalk, a structure formed in Pol I by the heterodimeric complex

Rpa43/Rpa14, which is involved in docking the essential Rrn3 initiation transcription factor to the enzyme (Peyroche *et al*, 2000; Yamamoto *et al*, 1996; Blattner *et al*, 2011). The Pol I-Rrn3 complex interacts with promoter bound factors, the core factor (CF), forming the initially transcribing complex (ITC) (Engel *et al*, 2017; Sadian *et al*, 2017; Han *et al*, 2017; Keener *et al*, 1998). Additionally, Pol I and Pol III contain subunits that are functionally and structurally related to Pol II-specific basal transcription factors, called the "Built-in Transcription Factors" (Kuhn *et al*, 2007; Geiger *et al*, 2010). Their presence in Pol I and Pol III results in a higher number of subunits, from 12 subunits in Pol II, to 14 and 17 for Pol I and Pol III, respectively, and correlates with substantial transcript production from a few genes (Werner, 2008). The heterodimer formed by Rpa34 and the N-terminal domain of Rpa49 (Rpa49Nt) in Pol I (*i.e.* Rpc53 and Rpc37 in Pol III) is related to the basal transcription factor TFIIF, and stimulates endogenous transcript cleavage activity (Geiger *et al*, 2010; Landrieux *et al*, 2006; Wu *et al*, 2011). Rpc34 in Pol III and the Rpa49 C-terminal domain (Rpa49Ct) bear a tandem winged helix motif similar to TFIIE (Geiger *et al*, 2010; Landrieux *et al*, 2006). Rpa49Ct binds DNA and is involved in initiation and elongation (Pilsl *et al*, 2016; Geiger *et al*, 2010). Finally, Rpa12 (Pol I) and Rpc11 (Pol III) C-terminal domains are both directly involved in stimulating endogenous transcript cleavage activity, similar to that of TFIIS for Pol II (Van Mullem *et al*, 2002; Kuhn *et al*, 2007).

Yeast genetic studies of Pol III and Pol I “Built-in Transcription Factors” have revealed striking differences, despite their clear similarities. Each Pol III subunit is essential for cell growth, but none of the Pol I “Built-in Transcription Factors" is needed for cell survival. Deletion of Rpa34 or invalidation of Rpa49Nt, by removing the TFIIF-like heterodimer, has a very mild growth effect *in vivo* (Gadal *et al*, 1997; Beckouet *et al*, 2008; Geiger *et al*, 2010). In contrast, full or C-terminal deletion of Rpa49 leads to a strong growth defect at all temperatures, which is more severe below 25°C (Liljelund *et al*, 1992; Beckouet *et al*, 2008;

Geiger *et al*, 2010). Full deletion of Rpa12 leads to a strong growth defect at 25 and 30°C, and is lethal at higher temperatures (Nogi *et al*, 1993). Deletion of the C-terminal extension of Rpa12 abolishes stimulation of intrinsic cleavage, without any detectable growth defect (Van Mullem *et al*, 2002; Kuhn *et al*, 2007). Finally, yeast strains carrying the triple deletion of *RPA49*, *RPA34* and *RPA12* are viable, but accumulate the growth defects associated with each of the single mutants (Gadal *et al*, 1997).

Pol I is functional in the absence of Rpa49, but shows well-documented initiation and elongation defects, both *in vivo* and *in vitro* (Liljelund *et al*, 1992; Beckouet *et al*, 2008; Albert *et al*, 2011; Pilsl *et al*, 2016; Gadal *et al*, 2002; Huet *et al*, 1975). Restoration of active rRNA synthesis, in the absence of Rpa49, has been used to identify factors involved in initiation and elongation, such as Hmo1 and Spt5, or other Pol I subunits, such as Rpa43 (Gadal *et al*, 2002; Beckouet *et al*, 2008; Viktorovskaya *et al*, 2011). We made use of the spontaneous occurrence of extragenic suppressors of the growth defect of the *rpa49* null mutant (Liljelund *et al*, 1992) to better understand the role of this subunit and reveal new interactions between the various subunits of RNA pol I during transcription. We showed that the suppressing phenotype was caused by specific point mutations in the two largest Pol I subunits, Rpa190 and Rpa135. We identified a small area at the interface between the jaw and lobe modules of the two largest subunits, in which the Rpa12 linker domain is inserted, by mapping the mutations onto the structure of Pol I. Rpa12 turned out to be essential for suppression. Moreover, Pol I carrying a single point mutation in Rpa12 was able to correct the growth defect and initiate transcription in the absence of Rpa49. Overall, our genetic data, gathered in the absence of Rpa49 or Rpa49Ct domain, suggest that the jaw/lobe interface, including the N-terminus of Rpa12, is important for the stabilization of Pol I that allows efficient transcription.

Results

Isolation of extragenic suppressor mutants of the growth defect in absence of Rpa49

We characterized extragenic suppressors of the *RPA49* deletion to better understand how cell growth is achieved in the absence of Rpa49. *RPA49* full-deletion mutants show a strong growth defect at 30°C and are unable to grow at 25°C. However, spontaneous suppressors have been previously observed (Liljelund *et al*, 1992). We reproduced this observation and quantified the frequency of occurrence of individual clones able to grow at 25°C. There was a low frequency of colony occurrence, comparable with the spontaneous mutation rate of a single control gene (*CAN1*; $< 5.10^{-6}$). We isolated more suppressors by irradiating the cells with UV light. UV irradiation, resulting in a survival rate of approximately 50%, increased the frequency of suppressor mutations by approximately 10 fold. We identified clones that grew at 25°C after three days and selected individual colonies, called SGR for suppressor of growth defect of *RPA49* deletion, with various growth rates. We ranked SGR from 1 to 186 based on their growth rates at 25°C; *SGR1* had a growth rate comparable to the wild-type (WT) condition (Figure 1A). We crossed the 186 SGR clones with a strain of the opposite mating type bearing only the deletion of *RPA49* to obtain diploid cells homozygous for the *RPA49* deletion and heterozygous for each suppressor. The restoration of growth of the diploids at 25°C showed that all suppressor phenotypes obtained were fully or partially dominant. We focused on the most efficient suppressor clones, SGR1 and SGR2, and performed tetrad analysis to follow segregation of the observed suppression phenotype. Each suppressor phenotype was linked to a single locus in the genome and neither SGR mutant had a strong growth defect (SGR1 in Figure 1A). We used global genomic mapping of SGR1 and SGR2, derived from "genetic interaction mapping" (GIM) methods (Decourty *et al*, 2008) (Materials and Methods; Suppl. Figure 1), and found a genomic linkage close to genes encoding the two largest Pol I subunits: *RPA135* for SGR1 and *RPA190* for SGR2 (Suppl.

Figure 1). Sequencing of the genomic DNA revealed that SGR1 bears a double mutation, whereas SGR2 bears a single one (*RPA135-I218T/R379K* and *RPA190-A1557V* alleles, respectively). Furthermore, we identified an additional mutant, SGR3, in *RPA135*, *RPA135-R305L*. The heterogeneity of the growth induced by strong UV mutagenesis prevented suppressor cloning from the 183 remaining SGR clones.

We next used the dominant phenotype of these suppressors to isolate more alleles which suppress the deletion phenotype of Rpa49 in *RPA190* and *RPA135*. We constructed a library of randomly generated mutants (see Materials and Methods) by propagating plasmids bearing WT *RPA135* or *RPA190* in a mutagenic *E.coli* strain. After phenotypic selection of *rpa49*Δ mutants bearing a mutagenized Rpa190 or Rpa135 subunit at 25°C, each plasmid bearing a suppressor allele was extracted, sequenced, and re-transformed into yeast to confirm the suppressor phenotype. We thus isolated nine novel alleles of Rpa190 and 13 of Rpa135 that were able to restore growth of *rpa49* deletion mutant at 25°C (supplementary Table 1). We evaluated the suppression strength based on growth restoration at 25°C relative to WT growth, as for the original SGR strains. Suppressor alleles more effective than SGR1, 2, or 3 were identified using mutagenesis of Rpa190 or Rpa135 (suppl. Table 1). In conclusion, we identified novel alleles of the two largest Pol I subunits as extragenic suppressors of the *rpa49*Δ-associated growth defect.

Rpa190 and Rpa135 mutant alleles can bypass the need of Rpa49 for optimal growth

The growth of the strains bearing one of six alleles (*RPA190-E1274K*, *RPA190-C1493R*, *RPA190-L1262P*, *RPA135-R379G*, *RPA135-Y252H*, and *RPA135-F301S*) was evaluated by a 10-fold dilution test (Figure 1B), showing good suppression by all in the absence of Rpa49. Previous genetic studies have isolated other genetic backgrounds that alleviate the growth defect of *rpa49*Δ at 25°C, such as *rpa43-35,326* (Beckouet *et al*, 2008), decreased rDNA copy number (Albert *et al*, 2011), Hmo1 over-expression (Gadal *et al*, 2002), or Spt5

truncations (Viktorovskaya *et al*, 2011). For all these mutants, rRNA synthesis was only partially restored in the absence of Rpa49 and significant transcription defects remained. Here, we focused on the *RPA135-F301S* allele, the most effective growth suppressor of the Rpa49 deletion: the *rpa49*Δ *RPA135-F301S* double mutant grew almost as well at 25°C as the WT strain (Figure 1B). In the absence of Rpa49, Rpa34 does not associate with transcribing Pol I (Beckouet *et al*, 2008). The *rpa49*Δ*Ct* allele does not have the TFIIE-like module, including the tandem wing helix motif (corresponding to residues 187-415). In strains bearing the *rpa49*Δ*Ct* allele, the TFIIF module (Rpa34 and Rpa49Nt) remains associated with the polymerase (Liljelund *et al*, 1992; Beckouet *et al*, 2008). However, yeast bearing *rpa49*Δ*Ct* or *rpa49* full-deletion have a similar growth defect (Liljelund *et al*, 1992; Beckouet *et al*, 2008). We sought further insight into the effect of the suppressors by integrating the *RPA135-F301S* point mutation into the endogenous gene in three genetic backgrounds: WT, *rpa49*Δ (full deletion), or *rpa49*Δ*Ct*. The growth rate was determined in each of these yeast strains at 30°C, in the presence or absence of *RPA135-F301S*. The suppressor allele *RPA135-F301S* had no effect on growth in the WT strain (doubling time of 102 min). The doubling time was 180 min for the *rpa49*Δ strain and *RPA135-F301S* suppression restored growth to a doubling time of 135 min. We observed similar suppression on the *rpa49*Δ*Ct* background (data not shown).

Pol I bearing *RPA135-F301S* allele restores efficient rRNA synthesis in the absence of Rpa49Ct *in vivo*

We used yeast mutant cells with a low and stable number of rDNA repeats to better associate the growth phenotype of the *RPA135-F301S* allele to nascent rRNA synthesis and Pol I density on transcribed genes *in vivo*. Almost all rRNA genes in such strains are in the active state and transcribe their rRNA genes with a very high Pol I loading rate (Cioci *et al*, 2003; Albert *et al*, 2011). Accordingly, this genetic background is better suited to study variations in the number of polymerase molecules per rRNA gene, as the cells of these strains have a fixed

number of rRNA copies which are all in the open chromatin state. We generated three strains on this background (bearing *rpa49*Δ*Ct*, *RPA135-F301S*, or *rpa49*Δ*Ct RPA135-F301S* alleles) and determined the doubling time (Figure 2A) and *de novo* synthesis of rRNA (Figure 2B). The presence of the *RPA135-F301S* allele in Pol I effectively compensated the growth defect caused by the absence of Rpa49. Labeling of the nascent rRNA was performed using a 2-min pulse with ^{3}H adenine. We performed the labeling in three independent cultures because of heterogeneity in the cell cultures of the *rpa49*Δ*Ct* mutant. RNA synthesis was reduced approximately five-fold for *rpa49ΔCter*, even under permissive conditions (30°C) (compare Fig. 2B, lane 1 to lanes 2 to 5). Pol I activity in the presence of *RPA135-F301S* was similar to that of the WT enzyme in the absence of Rpa49Ct (compare Figure. 2B, lanes 5 and 6). Thus, *RPA135-F301S* appeared to restore rRNA production in the absence of Rpa49.

Rpa49 is involved in initiation and elongation. We evaluated Pol I density on transcribed genes by performing Miller spreads, the only technique that currently allows the counting of individual Pol I molecules on a single rRNA gene (Miller & Beatty, 1969; Albert *et al*, 2011). We previously showed that full deletion of *rpa49* resulted in a three-fold decrease of Pol I density per gene in the same genetic background (Miller & Beatty, 1969; Albert *et al*, 2011). Cells of the strain expressing the *rpa49*Δ*Ct* allele showed a four-fold decrease of Pol I density per gene (Figure 2C). Expression of the *RPA135-F301S* allele in the presence of Rpa49 or Rpa49Ct had no influence on Pol I density (Fig. 2C, *RPA135-F301S*). In contrast to strain *rpa49*Δ*Ct*, the double mutant *rpa49*Δ*Ct RPA135-F301S* showed significantly higher pol I occupancy (46 instead of 21 Pol I molecules per gene, on average). Indeed, the double mutant restored full rRNA production, although it exhibited only half of the WT Pol I density per gene.

Overall, these results show that the presence of the *RPA135-F301S* allele in a strain lacking Rpa49Ct restores rRNA synthesis to WT levels and increases Pol I density on rRNA genes, indicative of productive transcription initiation and rRNA synthesis.

Most suppressors are clustered in a hotspot of Pol I

Structural data of Pol I are now available, showing Pol I in an inactive form (Fernández-Tornero *et al*, 2013; Engel *et al*, 2013), complexes of Pol I and Rrn3 (Pilsl *et al*, 2016; Engel *et al*, 2016; Torreira *et al*, 2017), complexes of Pol I with other initiation factors (Engel *et al*, 2017; Han *et al*, 2017; Sadian *et al*, 2017), and in elongating forms (Neyer *et al*, 2016; Tafur *et al*, 2016), respectively. We mapped Rpa135 and Rpa190 residues that suppressed the growth defect of the mutant strain *rpa49ΔCt* onto the structure of WT Pol I in which the structure of Rpa49 was determined(Han *et al*, 2017) (Figure 3A). Most of the suppressor mutations which provided growth recovery (see supplementary table 1) appeared to be clustered at a specific interface between the two largest subunits, Rpa190 and Rpa135 (figure 3B), between the lobe (Rpa135 - salmon) and the jaw (Rpa190 - blue). This small region is characterized by the presence of a beta-strand in the structure of Rpa12 (Rpa12 – yellow: residues 46-51, Figure 3B), following four beta-strands of Rpa190, thus forming a shared five-strand anti-parallel beta-sheet. The Rpa12 beta-strand also faces the Rpa135 lobe domain (residue 252 to 315 of Rpa135), in which six independent mutations were found, including *RPA135-F301S*. Notably, Rpa135 contains a pattern of three amino acids "DSF" (D299, S300, F301), which are highly conserved among eukaryotic species. Notably, we found suppressor mutations for each of these three amino acids (see supplementary table 1). The side chains of the mutated residues are apparently involved in electrostatic interactions that stabilize this jaw/lobe interface (Figure 3C). Substituted residues resulted in destabilization of this interface (see supplementary table 1), suggesting a specific rearrangement of the interface lobe/jaw in each mutant.

Point mutations in Rpa12 suppress the growth defect when Rpa49 is missing

We then tested whether mutated alleles of *RPA12* itself could behave as suppressors by generating a library of randomly mutagenized *RPA12* (see Materials and Methods). Two dominant alleles (*RPA12-S6L* and *RPA12-T49A*) efficiently suppressed the growth defect of *rpa49*Δ and of *rpa49*Δ*Ct* (Figure 4A, not shown here for *rpa49*Δ*Ct*). However, these *RPA12* suppressor alleles did not fully restore WT growth when expressed in the *rpa49*Δ mutant (compare the size of the colonies in Figure 4A.). We integrated the *RPA12-S6L* point mutation into the genome at its native locus in a low rDNA-copy-number genetic background, with or without *rpa49Ct* deletion, and analyzed the restoration of rRNA synthesis by pulse labeling (Figure 4B) and Pol I loading by Miller spreading (Figure 4C). rRNA synthesis and Pol I loading were largely restored when *RPA12-S6L* was expressed in strain *rpa49*Δ*Ct*, similar to that for the *RPA135-F301S* mutant. The 3D structure of Pol I shows that *RPA12-S6L* and *RPA12-T49A* obtained by random mutagenesis are specifically located in the "hotspot" at the jaw/lobe interface. Threonine 49 of Rpa12 is located on the beta-strand (Rpa12 aa 46-51) (Figure 3B), facing residues D299, S300, and F301 of Rpa135, and Rpa190-E1274 (Figure 3B). This residue also appears to be highly conserved among eukaryotic species. The second mutation, *RPA12-S6L*, is located in the N-terminal domain of Rpa12. In conclusion, all point mutations in Rpa190, Rpa135, and Rpa12 detected in the hotspot domain of the jaw/lobe interface can substitute the requirement for Rpa49Ct *in vivo*.

Rpa14, Rpa34, and the expander/DNA mimicking loop of Rpa190, are not involved in the suppression phenotype

The structural determination of Pol I revealed the presence of an extended loop inside the DNA-binding cleft folded in a "expander/DNA mimicking loop" conformation when Pol I is in an inactive, dimeric form (Engel *et al*, 2013; Fernández-Tornero *et al*, 2013). This element is not found in Pol II or III. These residues are inserted between the four beta-strands of

Rpa190, corresponding to the mutation hotspot. A small deletion of this Rpa190 domain (1361-1390) results in a slight slow-growth phenotype (Fernández-Tornero *et al*, 2013). We determined whether the expander/DNA mimicking loop was responsible for the suppression phenotype. We generated a novel allele, *rpa190*Δ*loop* (deletion of residues 1342-1411), which had no associated growth defect (Figure 5A). We were unable to generate a viable double mutant when combining this mutation with the *rpa49* full deletion. Thus, the DNA-mimicking loop is required for Pol I activity in the absence of Rpa49. We next tested whether deletion of this loop influences suppression by the *RPA135-F301S* allele. Note that the *rpa190*Δ*loop* combined with *RPA135-F301S* has no phenotype. There was no difference in the growth of the *rpa49*Δ *RPA135-F301S* double mutant and that of the triple mutant *rpa49*Δ *RPA135-F301S rpa190*Δ*loop* (Figure 5A). Thus, the expander/DNA mimicking loop of Rpa190 is not required for suppression, but is required for the viability of the *rpa49* deletion mutant.

Rpa34 forming a heterodimer with Rpa49Nt, and Rpa14 being essential in absence of Rpa49, we also introduced *RPA135-F301S* into yeast strains lacking theses Pol I subunits (Figure 5B and C). The growth of *RPA135-F301S*/*rpa14*Δ and *RPA135-F301S*/*rpa34*Δ double mutants was not different from that of the single mutants. However, *RPA135-F301S* suppressed the growth defect of the viable double mutant, *rpa34*Δ *rpa49*Δ, lacking both Rpa49 and Rpa34, the heterodimer partner of Rpa49 (Figure 5B). The double deletion mutant lacking both Rpa49 and Rpa14 was not viable, similar to the *rpa190*Δ*loop rpa49*Δ double mutant (Gadal *et al*, 1997). Introduction of the suppressor *RPA135-F301S*, by genetic crossing, resulted in a triple mutant (*rpa14*Δ *rpa49*Δ *RPA135-F301S*) that could grow, but much more slowly (Figure 5C).

Overall, *RPA135-F301S* had no effect when combined with the single deletions *rpa190*Δ*loop*, *rpa34*Δ, or *rpa14*Δ. However, *RPA135-F301S* suppression of *rpa49*Δ-associated growth defect does not require Rpa190 DNA mimicking loop, Rpa34, or Rpa14.

Rpa12 is required for suppression of the *rpa49*Δ-associated growth defect

We next evaluated whether specific regions of Rpa12 may be involved in the suppression of the *rpa49*Δ-associated growth defect (Figure 6A). The C-terminal region of Rpa12 (TFIIS-like) is inserted towards the active center of Pol I to stimulate intrinsic cleavage activity but is displaced during productive initiation and elongation steps. C-terminal deletion of Rpa12 resulted in normal growth (Van Mullem *et al*, 2002) (Figure 6A- lane 2), although the *Rpa12*Δ*Ct* allele is unable to stimulate cleavage activity *in vitro* (Kuhn *et al*, 2007). Full deletion of *RPA12* resulted in a slight growth defect at 24°C, which was stronger at 30°C (Nogi *et al*, 1993) (Figure 6A-lane 3). In contrast, *rpa49* deletion resulted in a growth defect at 30°C, which was stronger at 24°C (Liljelund *et al*, 1992) (Figure 6A-lane 4). Combining *rpa12*Δ*Ct* with *rpa49*Δ resulted in a mildly synergistic phenotype, with a stronger growth defect at both 24°C and 30°C (Figure 6A – lane 5). The double mutant lacking both full Rpa12 and Rpa49 subunits was viable, but had a major growth defect (Gadal *et al*, 1997) (Figure 6A – lane 6).

Random mutagenesis of *RPA12* did not lead to the isolation of *RPA12* alleles containing suppressor mutations in the C-terminal domain. We explored whether the C-terminal extension of Rpa12 is necessary for suppression of the *rpa49*Δ phenotype by introducing the Rpa12 C-terminal truncation into the strain bearing both *rpa49*Δ and suppressor alleles *RPA12-S6L* or *RPA12-T49A*. Thus, *RPA12-S6L* and *RPA12-S6L*-Δ*Ct* resulted in similar suppression of the *rpa49*Δ growth defect (Figure 6B***).*** *RPA12-T49A* behaved similarly to *RPA12-S6L* (data not shown).

We then introduced the *RPA135-F301S* allele and assessed the suppression phenotype of the strain lacking Rpa49 at 25°C, with or without the entire Rpa12 subunit (Figure 6C). We constructed a strain with *RPA12* under the control of the regulatable pGAL promoter. The growth defect of *rpa49*Δ was completely suppressed by the *RPA135-F301S* allele when *RPA12* was expressed (Figure 6C, left panel), whereas suppression mediated by *RPA135-F301S* was completely abolished in its absence (Figure 6C, middle panel). Residual growth of the *rpa49 rpa12* double mutant was detectable after 10 days (Figure 6B, right panel) and was the same with or without the *RPA135-F301S* allele.

In conclusion, we show that Rpa12, particularly its N-terminal portion, is required for the suppression of the growth defect mediated by *RPA135-F301S* when Rpa49 is depleted.

Rpa12 is required for efficient promoter-dependent transcriptional activity *in vitro*

The suppressor mutants suggest a functional interaction between Rpa49 and Rpa12. The absence of Rpa49 or its C-terminal extension strongly reduced Pol I loading on rDNA genes (Albert *et al*, 2011; Beckouet *et al*, 2008); Figure 2C), indicating an initiation defect *in vivo*. The *in vitro* results of promoter-dependent transcription assays in the absence of Rpa49, particularly of Rpa49Ct, are consistent with the *in vivo* data, in which their absence results in an almost initiation-inactive form of the polymerase, whereas nonspecific RNA synthesis is not as strongly affected (Pilsl *et al*, 2016). Miller spread experiments have been previously performed for mutant strains lacking Rpa12 (Prescott *et al*, 2004), but Pol I occupancy of the rDNA genes was not analyzed, and is difficult to interpret due to the known instability of Rpa190 in the absence of Rpa12 (Van Mullem *et al*, 2002). However, it is possible to test whether subunit Rpa12 supports transcription initiation *in vitro*. We thus performed promoter-dependent transcription and non-specific transcription assays comparing Pol I, lacking Rpa12, to WT Pol I (Figure 7).

In vitro, transcription on tailed templates was significantly reduced in the absence of Rpa12 when the amount of Pol I was held constant (approximately 14% using 4 nM Pol relative to that of WT Pol I). In promoter-dependent transcription the reduction in transcription efficiency was much more pronounced (approximately 1.2% of that of WT Pol I) indicating that Rpa12 is involved in the initiation step.

Discussion

Here, we investigated how the growth of cells can improve in the absence of Rpa49. We showed that altering a very specific area of Pol I resulted in a functional Pol I molecule lacking this subunit. We propose that the mutated area, which includes a part of subunit Rpa12, undergoes a conformational change that supports the initiation of transcription.

Suppressor mutants are not at the Rrn3-Pol I stalk interface

Our previous studies suggested the specific involvement of Rpa49 in the association and dissociation of Rrn3 from the Pol I stalk (Albert *et al*, 2011; Beckouet *et al*, 2008)). Here, we show that genetically modified polymerases lacking Rpa49 or Rpa49Ct, with a single modified residue in Rpa190, Rpa135, or Rpa12, at a position diametrically opposed to the position that binds to Rrn3, can initiate transcription and that strains harboring them grow normally. We propose that there is a second important interface which is involved in Pol I recruitment to the rDNA gene, in addition to the interface between Rrn3 and the stalk.

The role of Rpa12 in suppression

The Rpa12 subunit is involved in stimulating the intrinsic cleavage activity of Pol I through a TFIIS-like domain at its C-terminus. Purified Pol I with Rpa12 lacking the C-terminal domain has no cleavage activity (Kuhn *et al*, 2007). Furthermore, the C-terminal domain of Rpa12 can contact the active site of the polymerase in the inactive conformation and is retrieved in both initiation competent and elongating forms of the polymerase. Direct evidence that cleavage is not involved in suppression of the growth defect came from the experiments showing a fully functional suppressor phenotype for *RPA12ΔCt-S6L*, which lacks the domain required for stimulating cleavage.

The N-terminal domain of Rpa12, at the surface of Pol I, is involved in the recruitment of the largest subunit, Rpa190, at 37°C (Van Mullem *et al*, 2002) and is required for docking of this

subunit to the enzyme. A linker region of Rpa12 connects the N-terminal module (Rpb9-like) at the surface of Pol I to the mobile C-terminal region (TFIIS-like) and is therefore indirectly required for cleavage. *In vitro*, purified Pol I that lacks Rpa12 has less activity than WT Pol I in promoter-dependent transcription assays. Mutations in other Pol I domains, such as deletions in Rpa34, Rpa14, or the Rpa190-DNA mimicking loop, did not influence suppression of the *rpa49* deletion growth defect by the *RPA135-F301S* allele. In contrast, the Rpa12 linker was absolutely required for efficient suppression. Accordingly, the *RPA135-F301S* allele was unable to restore efficient growth when Rpa12 was absent. Thus, Rpa12 and *RPA135-F301S* cooperate to support initiation if Rpa49 is absent.

Modification of the jaw/lobe interface facilitates DNA cleft closure

RNA polymerase I undergoes major conformational changes during the transcription cycle, mainly affecting the width of the DNA-binding cleft(Fernández-Tornero, 2018). During the initiation of transcription, the cleft aperture narrows from a semi-open configuration, as seen in cryo-EM structures of the enzyme bound to Rrn3 (Engel *et al*, 2016; Pilsl *et al*, 2016; Torreira *et al*, 2017), to a fully closed conformation observed in transcribing complexes (Engel *et al*, 2017; Han *et al*, 2017). This allows gripping of the transcription bubble inside the cleft (Figure 8A). Following Rrn3 release, DNA binding is further secured by the Rpa49-linker, which crosses the cleft from the lobe to the clamp, passing over the downstream DNA, and the Rpa49Ct domain, which binds the upstream DNA in the vicinity of the clamp (Han *et al*, 2017; Tafur *et al*, 2016).

Cleft closure is achieved by the relative movement of two structural units, located on opposite sides of the cleft, which pivot using five hinges(Fernández-Tornero *et al*, 2013). The unit consisting of the shelf and clamp modules is apparently rigid, whereas that consisting of the core and lobe modules, which is in the vicinity of the mutated residues of our study, undergoes internal rearrangements (Movie 1). The most prominent reorganization within this

latter unit affects the Rpa190 jaw domain, the outer rim of which shifts away from the DNA by approximately 3.7 Å, using the lobe/jaw interface as a hinge. This movement also involves the linker region of subunit Rpa12, which contains a beta-strand (residues 46-50) that completes a four-stranded beta-sheet in the Rpa190 jaw domain. As a result, a short alpha-helix within the Rpa12 linker region shifts its position by approximately 3.0 Å.

Possible roles of Rpa12 in regulating DNA cleft closure

Rearrangements in the jaw of Rpa190 and Rpa12 linker regions are likely essential to allow pivoting of the shelf-clamp unit against the core-lobe unit. Without such motion, cleft closure would be impossible (Movie 1). We propose that *RPA135-F301S* or *RPA12-S6L* favor DNA capture by increasing the flexibility of the lobe/jaw/Rpa12 interface of Pol I relative to that of the WT polymerase. Structural analysis suggests that the Rpa49Ct and its linker domains are involved in securing the closed cleft conformation (Tafur *et al*, 2016; Han *et al*, 2017). Cleft closure is likely destabilized in the *rpa49*Δ*Ct* mutant (Figure 8B). We propose that the Rpa12 linker domain contributes to the hinge in the lobe/jaw interface. Rpa12 may be involved in cleft-closure, which is necessary to guide the DNA towards the active center, or it may stabilize DNA bound Pol I. Our mutated Pol I probably captures DNA more efficiently than WT polymerase. This structural rearrangement is strongly suggested by our genetic data and the requirement of Rpa12 for promoter-dependent *in vitro* initiation. There is indirect evidence that similar domains are involved in the initiation of transcription of Pol II and Pol III. Rpb9 in Pol II is similar to the Rpa12-N-terminal module, but lacks the TFIIS domain. Rpb9 is required for proper start site selection and transcription fidelity (Hull *et al*, 1995; Walmacq *et al*, 2009). Furthermore, mutations in the lobe domain of Rpb2, adjacent to Rpb9, alter both Pol II–TFIIF binding and the transcription start site (Chen *et al*, 2007). For Pol III, TFIIS has been shown to stimulate transcription initiation *in vitro* and *in vivo* (Ghavi-Helm *et*

al, 2008). However, motion at the lobe/jaw interface during cleft closure is only detectable in Pol I.

Figure legends

Figure 1. Alleles of *RPA190* and *RPA135* suppress the growth defect of the *rpa49*Δ mutant at various levels. (A) The SGR1 mutant restores growth of the *rpa49*Δ mutant. Ten-fold serial dilutions of wild-type (WT), *rpa49*Δ single mutant, SGR1 single mutant, and SGR1/*rpa49*Δ double mutant strains were spotted on rich media to assess growth at 30 and 25°C for three days. (**B**) Ten-fold dilutions of WT and *rpa49*Δ compared to *rpa49*Δ carrying various plasmids: pGL190_3 (*RPA190-E1274K*), pGL190_11 (*RPA190-C1493R*), pGL190_23 (*RPA190-L1262P*), pGL135_6prim (*RPA135-R379G*), pGL135_54 (*RPA135-Y252H*), or pGL135_33 (*RPA135-F301S*). Growth was evaluated after three days at 25°C. The strains and plasmids used are listed in supplementary Tables 2 and 3, respectively.

Figure 2. The *RPA135-F301S* allele restores growth and rRNA synthesis, and modulates Pol I occupancy of rDNA genes in the absence of Rpa49Ct. (A) Doubling times of WT, *rpa49*Δ*Ct*, *RPA135-F301S*, and the *rpa49*Δ*Ct*/*RPA135-F301S* double mutant in a low copy number background (see supplementary table 2). (**B**) *In vivo* labeling of newly synthesized RNAs. WT (lane 1), *rpa49*Δ*Ct* (lanes 2-4), *RPA135-F301S* (Lane 5), and the *rpa49*Δ*Ct*/*RPA135-F301S* double mutant (Lane 6) were grown to an OD_{600} of 0.8. Cells were then pulse-labeled with [8-^{3}H] adenine for 2 min. Samples were collected, and total RNA extracted and separated by gel electrophoresis. (**C**) Representative Miller spreads of WT, *rpa49*Δ*Ct*, *RPA135-F301S*, and the *rpa49*Δ*Ct/RPA135-F301S* double mutant. Panels on the right of each micrograph show interpretive tracing of the genes. Polymerases that appear on the gene are shown on the tracing by black dots. The number of polymerases counted on the genes is indicated below. N represents the number of individual spread genes used for quantification (see Materials and Methods).

Figure 3. Mapping of the modified residues in Rpa190, Rpa135, and Rpa12 alleles on the structure of Pol I. (A) Two different views of the original initial transcribing complex model and its 14 different subunits (PDB 5W66(Han *et al*, 2017)). (B) Most mutated suppressor residues are clustered at the interface between the jaw (Rpa190, blue) and lobe (Rpa135, salmon) modules of Pol I. Note that Rpa12 (residue 46 to 51; yellow) is part of this interface. (C) Enlargement of the areas containing the modified residues (Rpa190-N863, -S1259, -L1262, -E1274, -C1493, Rpa135-Y252, D299, S300, F301, R305, and Rpa12-S6, T49) shown in panel B. The figure was prepared with Pymol using the crystal structure of Pol I PDB 4C3I (Fernández-Tornero *et al*, 2013)).

Figure 4. The *RPA12-S6L* allele restores growth and rRNA synthesis and modulates Pol I occupancy of rDNA genes in the absence of Rpa49Ct. (A) Ten-fold dilutions of the *rpa49*Δ mutant carrying various plasmids: an empty pRS316 plasmid (*rpa49*Δ), YCp50-26 bearing *RPA49* (WT), pRS316-A12-S6L (*RPA12-S6L)*, or pRS316-A12-T49A (*RPA12-T49A)*. Growth was evaluated after three days at 25°C or two days at 30°C. (**B**) *In vivo* labeling of newly synthesized RNA. For comparison, WT (lane 1) and *rpa49*Δ*Ct* (lanes 2) depicted in figure 2B are shown with the *RPA12-S6L* single mutant and the *rpa49*Δ*Ct/RPA12-S6L* double mutant. (**C**) Representative Miller spreads of WT, *rpa49*Δ*Ct*, *RPA12-S6L*, and the *rpa49*Δ*Ct/RPA12-S6L* double mutant.

Figure 5. Rpa14, Rpa34, and the DNA mimicking loop of Rpa190 are not required for suppression. Deletion of the DNA mimicking loop of Rpa190 (A) or *RPA34* (B) does not modulate the suppression activity of *RPA135-F301S*. (C) *RPA135-F301S* suppresses the synthetic lethality between *rpa14*Δ and *rpa49*Δ. Ten-fold serial dilutions were performed seeded onto rich media and growth evaluated after three days at 24°C.

Figure 6. *RPA12* alleles can modulate the *rpa49*Δ-associated growth defect. (A) Growth of the double mutants: *rpa49*Δ *rpa12*Δ*Ct*, or *rpa49*Δ combined with full depletion of *rpa12*. Depletion of Rpa12 was achieved using a *pGAL-RPA12* construct on glucose containing medium (strain OGT30-1c). Ten-fold serial dilutions of OGT30-1c bearing pRS316-A12 (WT), pRS316-A12-DCter expressing Rpa12 bearing a C-terminal deletion of residues 65-125 (*rpa12*Δ*Ct*), or an empty plasmid pRS316 (-*rpa12*) were seeded onto media. The growth of *rpa49*Δ combined with *RPA12* depletion was tested using strain OGT30-3c bearing pRS316-A12 (*rpa49*Δ), pRS316-A12-DCter (*rpa12*Δ*Ct rpa49*Δ), or an empty plasmid pRS316 (-*rpa12 rpa49*Δ). Growth was assessed after four days at 24 or 30°C. (**B**) The C terminus of Rpa12 is not required for suppression. Ten-fold serial dilutions of OGT30-1c (*RPA49*-WT), bearing pRS316-A12 (WT) or pRS316-A12-DCter (*rpa12*Δ*Ct*), and OGT30-3c (*rpa49*Δ), bearing pRS316-A12 (WT), pRS316-A12-DCter (*rpa12*Δ*Ct*), pRS316-A12-S6L (*RPA12-S6L*), or pTD10 (*RPA12-S6L-*Δ*C*) were seeded onto media. Growth was assessed after four days at 24°C. (**C**) Suppression activity of *RPA135-F301S* is abolished in the absence of Rpa12. *RPA12*, under a regulatable promoter (pGAL) was either expressed (+*RPA12; left panel*) on galactose containing medium or repressed (-*RPA12; right panel*) on glucose containing medium. Ten-fold serial dilutions of *RPA49-WT*, *rpa49*Δ, *RPA49-WT*, *RPA135-F301S*, or *rpa49*Δ *RPA135-F301S* were grown at 24°C. Depletion of *RPA12* abolishes the suppression activity of *RPA135-F301S* (compare the left to the middle and right panels). Extended incubation (right panel, 10 days) was used to detect growth of the double mutant -*RPA12 rpa49*Δ on plates.

Figure 7. Subunit Rpa12 supports *in vitro* Pol I transcription initiation and non-specific transcription. Tailed template assays (lane 1-3) and promoter-specific transcription (lane 4-6) were performed using 4 nM WT Pol I or 4 and 12 nM Pol I lacking Rpa12 (see Materials and Methods). Quantification relative to WT activity is shown for each lane.

Figure 8. Schematic representation of Pol I (**A**) Free monomeric Pol I with mobile Rpa49Ct and linker. (**B**) Initially transcribing complex (ITC) upon insertion of melted DNA in the presence of Rpa49 (purple). Rpa49Ct interacts with upstream DNA and the Rpa49-linker is folded, closing the cleft. Movements of Rpa12 and the jaw with respect to the lobe are indicated with arrows. (**C**) Pol I lacking Rpa49 is likely defective in stabilizing the closed conformation in the DNA-binding cleft, likely resulting in a looser grip on the DNA (red asterisks). (**D**) Suppressor mutations (green) facilitate movement of the jaw/lobe interface and gripping of the DNA by the Pol I enzyme, in the absence of Rpa49.

MATERIALS & METHODS

Plasmids and yeast strain constructions

The oligonucleotides used in this study are listed in supplementary Table 4. Plasmids and details of the cloning steps are described in supplementary Table 3. Randomly mutagenized *RPA190* and *RPA135* libraries were obtained by transformation and amplification of pVV190 and pNOY80, respectively, into XL1-red strains according to the manufacturer's guidelines (XL1-Red Competent Cells, from Agilent Technologies). Yeast strains are listed in supplementary Table 2, and were constructed by meiotic crossing and DNA transformation (Schiestl & Gietz, 1989)(Sambrook *et al*, 1989). The yeast media and genetic techniques were described previously (Sherman *et al*, 1986).

yCNOD226-1a was obtained from yCNOD223-2a by switching the *KAN-MX* to the *NAT-MX* marker under the control of the MF(ALPHA)2/YGL089C promoter (alphaNAT-MX4), which allowed selection of MATα haploid cells (Decourty *et al*, 2008). OGT9-6a is an offspring of yCNOD226-1a crossed with BY4741. OGT8-11a is an offspring of BY4742 crossed with Y1196. Strains OGT9-6a and OGT8-11a were plated on rich media and UV irradiated (5W/m^2 during 5 second), resulting in 50% survival. LH514D and LH11D are suppressor clones of the growth defect selected from UV-irradiated OGT9-6a grown at 25°C. AH29R is a suppressor clone of the growth defect selected from UV-irradiated OGT8-11a grown at 25°C. Genetic interaction mapping (GIM) analysis of the *RPA49* deletion mutant was performed as described previously (Decourty *et al*, 2008). Microarray data were normalized using MATLAB (MathWorks, Inc., Natick, MA) as previously described (Albert *et al*, 2011). OGT15-7b is an offspring of LH514D with BY4741, followed by homologous recombination using PCR-amplified fragments generated with oligos 1716 and 1717 and pCR4-HIS3 as template. yTD16-1a was first transformed with plasmid pCJPF4-GAL49-1. Then, *RPA135* was tagged by homologous recombination using PCR-amplified fragments generated with

oligos 835 and 836 and genomic DNA of strain *RPA135-TAP* or yTD6-6c, generating yTD27-1 and yTD28-1a, respectively. Strain yTD25-1a bears a C-terminal deletion of *RPA49* generated by homologous recombination using PCR-amplified fragments generated with oligos 208 and 1515 and pFA6-KAN-MX6 as template. yTD11-1a was derived from strain yTD25-1a after switching to HPH-MX by homologous recombination using pUC19-HPH cut by *Bam*HI. C-terminal deletion of *RPA49 in* yTD29-1a and yTD30-1a were generated by homologous recombination using PCR-amplified fragments generated with oligos 649 and 650 and yTD11-1 genomic DNA as template, transformed into yTD27-1 and yTD28-1a, respectively. Genomic allelic insertion of *RPA12-S6L* in yTD31-1a and yTD23-1a was performed by homologous recombination using PCR-amplified fragments generated with oligos 1556 and 1557 and pRS316-A12-S6L-KAN as template, transformed into yTD27-1 and yTD29-1a, respectively.

TGT135-3b was obtained after sporulation of y27138 transformed by pNOY80. TGT135-3b and OGT15-9d were mated to generate TGT12. yTD2-3b and yTD2-3d are offspring of TGT12 transformed with pGL135_33. yTD6-6c and yTD6-6b were generated by homologous recombination using pTD2_6c_135TAP cut with *Xho*I-*Nsi*I, transformed into yTD2-3b and yTD2-3d, respectively. yTD48-1a was generated by deletion of the Rpa190 DNA-mimicking loop using homologous recombination with PCR-amplified fragments generated using oligos 1189 and 1194 and genomic DNA of strain SCOC2260 as template, transformed into BY4741.

yTD51-2c, yTD51-8a, and yTD51-5a are offspring of yTD48-1a mated with yTD37-3a. yTD36-2b is an offspring of yCN224-1a mated with yTD40-1a. yTD37-3d and yTD37-7d are offspring of yCN224-1a mated with yTD41-1a. yTD38-3d is an offspring of yCN225-1a mated with yTD40-1a and yTD39-8a is an offspring of yCN225-1a mated with yTD41-1a.

Strain yTD53-1a was constructed by homologous recombination using a PCR-amplified fragment generated with oligos 1634 and 1635 and pFA6a-KanMX6-GAL::3HA as template. OGT30-1a and OGT30-3a are offspring of yTD53-1a mated with yTD6-6b. yTD40-1a and yTD41-1a were generated by homologous recombination using PCR-amplified fragments generated with oligos 700 and 1679 and pFA6a-HA-KlURA3 as template, transformed into OGT30-3a and OGT30-1a respectively, switching *RPA135-TAP*-tag to untagged *RPA135*.

In vivo labeling and RNA extraction and analysis

Metabolic labeling of pre-rRNA was performed as previously described (Hermann-Le Denmat *et al*, 1994) with the following modifications. Strains were pre-grown in synthetic glucose-containing medium lacking adenine at 30°C to an OD_{600} of 0.8 at. One milliliter cultures were labeled with 50 µCi [8-^{3}H] adenine (NET06300 PerkinElmer) for 2 min. Cells were collected by centrifugation and the pellets frozen in liquid nitrogen. RNA was then extracted as previously described (Beltrame & Tollervey, 1992) and precipitated with ethanol. For high molecular weight RNA analysis, 20% of the RNA was glyoxal denatured and resolved on a 1.2% agarose gel. Low molecular weight RNAs were resolved on 8% polyacrylamide/8.3 M urea gels.

Miller spread experiments and analysis

Chromatin spreading was mainly performed as described previously with minor modifications (Osheim *et al*, 2009). Carbon-coated grids were rendered hydrophilic by glow discharge instead of ethanol treatment. Negatively stained chromatin was obtained by short incubation with heavy metal followed by quick drying of the sample. Images were obtained using a JEOL JEM-1400 HC electron microscope (40 to 120 kV) with an Orius camera (11Mpixels). The position of the RNA polymerase I molecules and the rDNA fiber were determined by

visual inspection of micrographs using Image J (http://rsb.info.nih.gov/ij/). Digital images were processed by software programs Image J and Adobe Photoshop® (v. CS6).

In vitro promoter-dependent transcription assays

In vitro promoter-dependent transcription reactions were performed as previously described (Pilsl *et al*, 2016; Tschochner, 1996) with some modifications. Briefly, 1.5 ml reaction tubes (Sarstedt safety seal) were placed on ice. Template (0.5 –1 µl; 50–100 ng DNA) was added, corresponding to a final concentration of 5–10 nM per transcription reaction (25-µl reaction volume). Core factor (1–2 µl; 0.5 to 1 pmol/µl; final concentration 20–40 nM) and 1–3 µl Pol I (final concentration 4–12 nM) were added to each tube. Then, 20 mM HEPES/KOH pH 7.8 was added to a final volume of 12.5 µl. Transcription was started by adding 12.5 µl 2X transcription buffer. The samples were incubated at 24°C for 30 min at 400 rpm in a thermomixer. Transcription was stopped by adding 200 µl Proteinase K buffer (0.5 mg/ml Proteinase K in 0.3 M NaCl, 10 mM Tris/HCl pH 7.5, 5 mM EDTA, and 0.6% SDS) to the supernatant. The samples were incubated at 30°C for 15 min at 400 rpm in a thermomixer. Ethanol (700 µl) p.a. was added and the tubes mixed. Nucleic acids were precipitated at -20°C overnight or for 30 min at -80°C. The samples were centrifuged for 10 min at 12,000g and the supernatant removed. The precipitate was washed with 0.15 ml 70% ethanol. After centrifugation, the supernatant was removed and the pellets dried at 95°C for 2 min. RNA in the pellet was dissolved in 12 µl 80% formamide, 0.1 M TRIS-Borate-EDTA (TBE), 0.02% bromophenol blue, and 0.02% xylene cyanol. Samples were heated for 2 min with vigorous shaking at 95°C and briefly centrifuged. After loading on a 6% polyacrylamide gel containing 7M urea and 1X TBE, RNAs were separated by applying 25 watts for 30–40 min. The gel was rinsed in water for 10 min and dried for 30 min at 80°C using a vacuum dryer. Radiolabelled transcripts were visualised using a PhosphoImager.

Suppl movie legends 1

Supplemental Movie 1. Conformational changes in Pol I upon initiation. The movie starts with the closed cleft conformation (PDB 5W66 (Han *et al*, 2017)), in which melted DNA occupies the cleft and then changes to the intermediate cleft conformation observed in monomeric Pol I (PDB 5M3M(Neyer *et al*, 2016)). Relevant structural regions have been variously colored and labeled, and residues mutated in this report are shown in red.

Supplementary tables

Sub.	Allele	Strength	Hotspot	Location	Mutant effect
Rpa190	N863T	Weak	Funnel	Funnel/ Rpa12-linker	Destabilization of Funnel/Rpa12
Rpa190	S1259L	Medium	Jaw	Jaw/Shelf hinge	Hinge conformation
Rpa190	L1262P	Weak	Jaw	Jaw/Shelf hinge	Hinge conformation
Rpa190	E1274K	Medium	Jaw	Jaw/ Rpa12-linker interface	Destabilization of Jaw/Rpa12
Rpa190	C1493R	Medium	Jaw	Jaw/ Rpa12-linker interface	Destabilization of Jaw/Rpa12
Rpa135	Y252H	Strong	Lobe	Jaw/Lobe interface	Destabilization of Jaw/Lobe
Rpa135	D299G	Medium	Lobe	Jaw/Lobe interface	Destabilization of Jaw/Lobe
Rpa135	S300F	Medium	Lobe	Jaw/Lobe interface	Destabilization of Jaw/Lobe
Rpa135	F301S	Strong	Lobe	Jaw/Lobe interface	Destabilization of Jaw/Lobe
Rpa135	F301L	Strong	Lobe	Jaw/Lobe interface	Destabilization of Jaw/Lobe
Rpa135	**SGR3** R305L	Medium	Lobe	Jaw/Lobe interface	Destabilization of Jaw/Lobe
Rpa12	S6L	Medium	N-terminal	Jaw/ Rpa12-linker interface	Destabilization of Jaw/Rpa12
Rpa12	T49A	Medium	Linker	Jaw/ Rpa12-linker interface	Destabilization of Jaw/Rpa12
Rpa190	L608S	Medium			
Rpa190	E611K	Medium			
Rpa190	S936A	Weak			
Rpa190	**SGR2** A1557V	Weak			
Rpa135	D157G	Medium			
Rpa135	D157N	Medium			
Rpa135	**SGR1** I218/ R379K	Medium			
Rpa135	R379G	Strong			
Rpa135	G580D	Medium			
Rpa135	C584Y	Weak			
Rpa135	I913V	Medium			

Supplementary table 1. List of 24 individual suppressor mutations of the growth defect of *rpa49*Δ strain in the Rpa190, Rpa135, and Rpa12 subunits (Sub.). The suppressors were classified according to growth rate when combined with *rpa49*Δ mutant: weak, medium, or strong. SGR1, 2, and 3 depict alleles originally isolated after UV mutagenesis (see text). Thirteen of the 24 mutants, affecting 12 different positions, were found in a specific hot-spot shown in Figure 4.

Supplementary table 2: Yeast strains used in this study

Referred to as	strain	Genotype	source
WT in figures 1 and 5	*BY4741*	*MATa his3Δ1 leu2Δ0 met15Δ0 ura3Δ0*	*Euroscarf*
	BY4742	*MATalpha his3Δ1 leu2Δ0 lys2Δ0 ura3Δ0*	*Euroscarf*
	y1196	*MATa his3Δ1 leu2Δ0 lys2Δ0 ura3Δ0 rpa49Δ::KANMX4*	*Euroscarf*
	y27138	*MATa/alpha his3Δ1/his3Δ1 leu2Δ0/leu2Δ0 ura3Δ0/ura3Δ0 lys2Δ0/LYS2 MET15/met15Δ0 rpa135Δ::KANMX4/RPA135*	*Euroscarf*
	TGT135-3b	*MATa his3Δ11 leu2Δ0 ura3Δ0 lys2Δ0 rpa135Δ::KANMX4 +pNOY80*	*Euroscarf*
	TGT12	*MATa/alpha his3Δ1/his3Δ1 leu2Δ0/leu2Δ0 ura3Δ0/ura3Δ0 lys2Δ0/lys2Δ0 rpa135Δ::KANMX4/RPA135 rpa49Δ::HPHMX4/RPA49*	*Euroscarf*
rpa49Δ in figure 1, with the plasmids indicated in the legend	*OGT9-6a*	*MATalpha his3Δ1 leu2Δ0 met15Δ0 ura3Δ0 rpa49Δ::alphaNATMX6*	*This study*
rpa49Δ in figure 4A, with the plasmids indicated in the legend	*OGT8-11a*	*MATa his3Δ1 leu2Δ0 lysΔ0 ura3Δ0 rpa49Δ::KANMX6*	*This study*
SGR1 in figure 1	*OGT15-7b*	*MATa his3Δ1 leu2Δ0 lysΔ0 ura3Δ0 HIS3::RPA135(I218T, R379K)*	*This study*
SGR1 rpa49Δ in figure 1	*LH514D*	*MATalpha his3Δ1 leu2Δ0 met15Δ0 ura3Δ0 rpa49Δ-alphaNAT RPA135(I218T, R379K)*	*This study*
SGR2	*AH29R*	*MATa his3Δ1 leu2Δ0 lysΔ0 ura3Δ rpa49Δ- kanmx4 RPA190-1557V*	*This study*
SGR3	*LH11D*	*MATalpha his3Δ1 leu2Δ0 met15Δ0 ura3Δ0 rpa49Δ-alphaNAT RPA135-R305L*	*This study*
	RPA135-TAP	*MATalpha his3Δ1 leu2Δ0 met15Δ0 ura3Δ0 RPA135-TAP::HIS3MX6*	*202233825* (Ghaemmaghami *et al*, 2003)
	yTD16-1a	*MATa ade2-1 ura3-1 his3-11,15 trp1-1 leu2-3,112 can1-100 fob1{Delta}::NAT-MX, rDNA copy no. ~25*	*This study*
WT in figures 2, 4B, and 4C	*yTD27-1a*	*MATa ade2-1 ura3-1 his3-11,15 trp1-1 leu-3,112 can1-100 fob1Δ::NAT-MX RPA135-TAP-HIS3, rDNA copy number ~25 + pCJF4-LEU-GAL49*	*This study*
RPA135-F301S in figure 2	*yTD28-1a*	*MATa ade2-1 ura3-1 his3-11,15 trp1-1 leu-3,112 can1-100 fob1Δ::NAT-MX RPA135-F301S-TAP-HIS3, rDNA copy number ~25, + pCJF4-LEU-GAL49*	*This study*
	yTD25-1a	*MATa his3Δ1 leu2Δ0 met15Δ0 ura3Δ0 rpa49ΔC(186-416)::KAN-MX4*	*This study*
	yTD11-1a	*MATa his3Δ1 leu2Δ0 met15Δ0 ura3Δ0 rpa49ΔC(186-416)::HPH-MX4*	*This study*
rpa49ΔCt in figures 2,4B, and 4C	*yTD29-1a*	*MATa ade2-1 ura3-1 his3-11,15 trp1-1 leu-3,112 can1-100 fob1Δ::NAT-MX RPA135 -TAP-HIS3 rpa49ΔC(186-416)::HPH, rDNA copy number ~25, + pCJF4-LEU-GAL49*	*This study*
rpa49ΔCt RPA135-F301S in figure 2	*yTD30-1a*	*MATa ade2-1 ura3-1 his3-11,15 trp1-1 leu-3,112 can1-100 fob1Δ::NAT-MX RPA135-F301S-TAP-HIS3 rpa49ΔC(186-416)::HPH, rDNA copy number ~25, + pCJF4-LEU-GAL49*	*This study*
RPA12-S6L in figures 4B and 4C	*yTD31-1a*	*MATa ade2-1 ura3-1 his3-11,15 trp1-1 leu-3,112 can1-100 fob1Δ::NAT-MX RPA135- TAP-HIS3 RPA12-S6L-KAN-MX, rDNA copy number ~25, + pCJF4-LEU-GAL49*	*This study*
rpa49ΔCt RPA12-S6L in figure 4B.	*yTD23_1a*	*MATa ade2-1 ura3-1 his3-11,15 trp1-1 leu-3,112 can1-100 fob1Δ::NAT-MX RPA135- TAP-HIS3 RPA12-S6L-KAN-MX rpa49ΔC(186-416)::HPHMX, rDNA copy number ~25*	*This study*
rpa49Δ in figures 6 and 7	*OGT15-9d*	*MATalpha his3Δ1 leu2Δ0 lysΔ0 ura3Δ0 rpa49Δ::HPHMX*	*This study*
	SCOC2260	*Mata ade2 arg4 leu2-3,112 trp1-289 ura3-52 RPB6::TAP-K.L.URA3 rpa190-ΔLOOP-KANMX*	*This study*

Supplementary table 2 (continued)

rpa190Δloop in figure 5A	*yTD48-1a*	*MATa his3Δ1 leu2Δ0 lysΔ0 ura3Δ0 rpa190Δloop::KANMX*	*This study*
rpa190Δloop RPA135-F301S in figure 5A	*yTD51-2c*	*MATalpha his3Δ1 leu2Δ0 met15Δ0 ura3Δ0 lys2Δ0 rpa190Δloop::KANMX RPA135-F301S-URA3Kl*	*This study*
rpa190Δloop RPA135-F301S rpa49Δ in figure 5A	*yTD51-8a*	*MATa his3Δ1 leu2Δ0 lys2Δ0 met15Δ0 ura3Δ0 RPA135-F301S-URA3Kl rpa49Δ::HPHMX*	*This study*
RPA135-F301S rpa49Δ in figure 5A	*yTD51-5a*	*MATa his3Δ1 leu2Δ0 lysΔ0 ura3Δ0 rpa49Δ::HPHMX*	*This study*
rpa49Δ in figures 5B and 5C	*yCN223-2a*	*MATalpha his3Δ1 leu2Δ0 met15Δ0 ura3Δ0 lys2Δ0 rpa49Δ::KANMX*	*This study*
	yTD2-3b	*MATa ura3Δ0 his3-Δ1 leu2-Δ0 lys2-Δ0 rpa135::KANMX, pGL135_33 (ARS/CEN URA3 RPA135-F301S)*	*This study*
rpa49Δ RPA135-F301S in figures 5B and 5C	*yTD2-3d*	*MATa his3Δ1 leu2Δ ura3Δ0 lys2Δ0 rpa135Δ::KANMX rpa49Δ::HPHMX + pGL135_33 (ARS/CEN RPA135-F301S)*	*This study*
	yCN224-1a	*MATalpha his3Δ1 leu2Δ0 met15 ura3Δ0 lys2Δ0 rpa34Δ -KAN-MX*	*This study*
rpa34Δ in figure 5B	*yCN224-1a*	*MATalpha his3Δ1 leu2Δ0 met15Δ0 ura3Δ0 lys2Δ0 rpa34Δ::KANMX*	*This study*
rpa34Δ RPA135-F301S in figure 5B	*yTD36-2b*	*MATalpha his3Δ1 leu2Δ0 ura3Δ0 lys2Δ0 rpa34Δ::NATMX RPA135-F301S::URA3*	*This study*
rpa34Δ rpa49Δ in figure 5B	*yTD37-7d*	*MATalpha his3Δ1 leu2Δ0 ura3Δ0 lys2Δ0 rpa34Δ::NATMX rpa49Δ::HPHMX*	*This study*
rpa34Δ rpa49Δ RPA135-F301S in figure 5B	*yTD37-3d*	*MATalpha his3Δ1 leu2Δ0 ura3Δ0 lys2Δ0 rpa34Δ::NATMX rpa49Δ::HPHMX RPA135-F301S::URA3*	*This study*
	yCN225-1a	*MATalpha his3Δ1 leu2Δ0 MET15 ura3Δ0 lys2Δ0 rpa14Δ -KAN-MX*	*This study*
rpa14Δ in figure 5C	*yCN225-1a*	*MATalpha his3Δ1 leu2Δ0 lysΔ0 ura3Δ0 rpa14Δ:: KANMX*	*This study*
rpa14Δ RPA135-F301S in figure 5C	*yTD38-3d*	*MATa his3Δ1 leu2Δ0 ura3Δ0 lys2Δ0 rpa14Δ::NATMX RPA135-F301S::URA3*	*This study*
rpa14Δ rpa49Δ RPA135-F301S in figure 5C	*yTD39-8a*	*MATa his3Δ1 leu2Δ0 ura3Δ0 lys2Δ0 rpa14Δ::NATMX rpa49Δ::HPHMX RPA135-F301S::URA3*	*This study*
	yTD53-1a	*MATalpha his3Δ1 leu2Δ0 lys2Δ0 ura3Δ0 KANMX6-pGAL::RPA12*	*This study*
RPA12 alleles in figure 6 with the plasmids indicated in the legend	*OGT30-1c*	*MATa his3Δ1 leu2Δ0 lysΔ0 ura3Δ0 KANMX-pGAL::RPA12*	*This study*
rpa49Δ in Figure 6 with the plasmids indicated in the legend	*OGT30-3c*	*MATalpha his3Δ1 leu2Δ0 lysΔ0 ura3Δ0 rpa49Δ:: HPHMX KANMX-pGAL::RPA12*	*This study*
	OGT30-1a	*MATa ura3-Δ0 his3-Δ1 leu2-Δ0 lys2-Δ0 rpa49Δ::HPH RPA135-(F301S)-TAP-HIS3 KANMX-pGAL::RPA12*	*This study*
	OGT30-3a	*MATa ura3-Δ0 his3-Δ1 leu2-Δ0 lys2-Δ0 RPA135-(F301S)-TAP -HIS3 KANMX-pGAL::RPA12*	*This study*
	yTD40-1a	*MATa ura3-Δ0 his3-Δ1 leu2-Δ0 lys2-Δ0 RPA135-(F301S)-STOP-URA3 KANMX-pGAL::RPA12*	*This study*
	yTD41-1a	*MATa ura3-Δ0 his3-Δ1 leu2-Δ0 lys2-Δ0 rpa49Δ::HPH RPA135-(F301S)-STOP-URA3 KANMX-pGAL::RPA12*	*This study*
RPA135-F301S in figure 6B	*yTD42-1a*	*MATa his3Δ1 leu2Δ0 lysΔ0 ura3Δ0 RPA135-F301S::URA3 KANMX-pGAL::RPA12*	*This study*
rpa49Δ RPA135-F301S in figure 6B	*yTD43-1a*	*MATalpha his3Δ1 leu2Δ0 lysΔ0 ura3Δ0 rpa49Δ:: HPHMX RPA135-F301S::URA3 KANMX-pGAL::RPA12*	*This study*
WT in figure 7	*yJPF159-1a*	*MATa his3Δ1 leu2Δ0 lys2- ura3Δ0 RPA135-TEV-ProtA::KANMX6*	*This study*
rpa12 in figure 7	*yJPF165-1a*	*MATa his3Δ1 leu2Δ0 lys2- ura3Δ0 RPA135-TEV-ProtA::KANMX6 HIS3MX::GAL::HA-RPA12*	*This study*

Supplementary table 3: Plasmids used in this study

Name	Description	Source
pUC19-HPH	*Plasmid bearing HPH-MX4*	(Berger *et al*, 2007)
pFA6-kanMX6	*Plasmid bearing KAN-MX6*	(Longtine *et al*, 1998)
pFA6a-KanMX6-GAL::3HA	*Plasmid used for GAL promoter insertion*	(Longtine *et al*, 1998)
pFA6a-HA-KlURA3	*Plasmid used for epitope switching*	(Sung *et al*, 2008)
pNOY80	*Plasmid CEN6 ARS4, URA3, RPA135*	(Yano *et al*, 1992)
pVV190	*Plasmid pFL44-A190 (2µ URA3 RPA190)*	(Van Mullem *et al*, 2002)
pRS316	*CEN6 ARS4, URA3*	(Sikorski & Hieter, 1989)
pCR4-HIS3	*HIS3*	(Sikorski & Hieter, 1989) (Berger *et al*, 2008)
pGL190_3	*(2µ URA3 RPA190-E1274K) selected from randomly mutagenized p*VV190	This study
pGL190_11	*(2µ URA3 RPA190- C1493R) selected from randomly mutagenized p*VV190	This study
pGL190_23	*(2µ URA3 RPA190- L1262P) selected from randomly mutagenized p*VV190	This study
pGL135_6prim	*(CEN4 URA3 RPA135-R379G selected from randomly mutagenized p*NOY80	This study
pGL135_54	*(CEN4 URA3 RPA135-Y252H) selected from randomly mutagenized p*NOY80	This study
pGL135_33	*(CEN4 URA3 RPA135-F301S) selected from randomly mutagenized p*NOY80	This study
pTD1_3b_135TAP	*Plasmid pNOY80 bearing RPA135-TAP-HIS3 obtained by homologous recombination using a PCR-amplified fragment generated with oligos 835 and 836 and genomic DNA of strain 202233825 as template.*	This study
pTD2_6c_135TAP	*Plasmid pNOY80 bearing RPA135-F301S-TAP-HIS3 obtained by homologous recombination using a PCR-amplified fragment generated with oligos 835 and 836 and genomic DNA of strain 202233825 as template.*	This study
pTD5	*Plasmid pTD1_3b_135TAP deleted of URA3 using NsiI and SdaI digestion and self-ligation.*	This study
pTD6	*Plasmid pTD2_6c_135TAP deleted of URA3 using NsiI and SdaI digestion and self-ligation.*	This study
Ycp50-26	*URA3 ARS/CEN RPA49*	P. Thuriaux, unpublished(Sikorski & Hieter, 1989)
pRS316-A12	*pRS316 vector ligated with a PCR-generated fragment using oligos 1554 and 1555 and yeast genomic DNA as template cut BamHI-XbaI, and cloned at same site.*	This study
pRS316-A12-AvrII	*PCR mediated mutagenesis to introduce AvrII site in* pRS316-A12 using oligos 1714 and 1715.	This study
pRS316-A12-S6L	*S6L Allele of RPA12 isolated as a suppressor of the rpa49Δ growth defect, selected from a PCR-mediated random mutagenesis of* pRS316-A12-AvrII.	This study
pRS316-A12-S6L-KAN	*Plasmid obtained using* pRS316-A12-S6L *modified by homologous recombination using a PCR-amplified fragment generated with oligos 1682 and 1559 and* pFA6-kanMX6 *as template.*	This study
pRS316-A12-T49A	*T49A Allele of RPA12 isolated as a suppressor of the rpa49Δ growth defect, selected from a PCR mediated random mutagenesis of* pRS316-A12-AvrII.	This study
pRS316-A12-DCter	*Plasmid obtained using* pRS316-A12 *modified by homologous recombination using a PCR-amplified fragment generated with* oligos *1371 and 1559 and* pFA6-kanMX6 *as template.*	This study
pTD9	*Plasmid obtained using* pRS316-A12-T49A *modified by homologous recombination using a PCR-amplified fragment generated with* oligos *1371 and 1559 and* pFA6-kanMX6 *as template.*	This study
pTD10	*Plasmid obtained using* pRS316-A12-S6L *modified by homologous recombination using a PCR-amplified fragment generated with* oligos *1371 and 1559 and* pFA6-kanMX6 *as template.*	This study

pCJPF4	*pFL36cII with LEU2 marker, CEN4, containing RPA49 coding region*	This study
pCJPF4-GAL49-1	*Plasmid obtained using pCJPF4 modified by homologous recombination using a PCR-amplified fragment generated with* oligos *624 and 625 and* pFA6a-KanMX6-GAL::3HA *as template.*	This study
pMAX1	*Plasmid including Pol I promoter used for in vitro assays*	(Pilsl *et al*, 2016)
pUC 19 tail g- TER elongated	*Plasmid containing tailed template DNA containing 18 S rDNA for non-specific in vitro transcription*	(Merkl *et al*, 2014)

Supplementary table 4: Oligonucleotides used in this study

Sequence	N°
gctgctttatagaaccatctagcaaaaaaaaaaaccagagcaaaccaaatgctcagtatatacctctaggtaactgaattcgagctcgtttaaac	208
ccactattgcagtcgttatcaacctttgcactttatctagtagaattcgagctcgtttaaac	624
cactttcaatttcgatttcagaaacagacctttcacggacattttgagatccgggtttt	625
catagtttctggcatgaccc	649
gaagaatcctggtagtatgg	650
tcgatgaattcgagctcgt	700
gacgctgatgacatcgagtg	835
tgatgggcacatatgaagtc	836
aggttctaacgttaatgtttctcaa	1189
actttataataccctagctctctta	1194
aagtcacaattctccaatttaaaagtcgtcaccacgacggcagacgatgcgtttccatcttctcttagagccaagaaatgaggcgcgccacttctaaa	1371
ctacgttcgacttatacaaaaaaaagaagtctgaaaaggacgaattcgtattacacggtgaaaacgagagactagaataccggatccccgggttaattaa	1515
gggggatcctttcaaatattgctataaaaatggatgatagc	1554
cgctctagacactgaatgtcacgatagagttatc	1555
cactgaatgtcacgatagagttatcgctgt	1556
tttcaaatattgctataaaaatggatgata	1557
tctatagatgttcacatgatgaaagcggggatgatattaatgtacaaattgtaatatgtgcgaacacaacccaatcagaattcgagctcgtttaaac	1559
ctaatacggcattaggattttccaggagatcaccacagtccaagcaaaaaattaacgatcctacaacagacattttgagatccgggtttt	1634
tttatgtcaagtgaagggcattgcatggcaagtgtaaagaatccaagaaggaattcgagctcgtttaaac	1635
agttaagatctgcagatgaaggtgctactgtcttctatacatgcacttcctgtggttacaagttccgtaccaacaattgatgaggcgcgccacttctaaa	1682
ttgaagtacttggactctgagctatccgcaatgggtataagattgcgttataatgtagagcccaaataacggatccccgggttaattaa	1679
gatctcctggaaaatcctaatgccgtcctaggctctaacgttgaatgcagcc	1714
ggctgcattcaacgttagagcctaggacggcattaggattttccaggagatc	1715
gatttgtttaacggcttctttgtagtcatcctgctgttgtttttgtatgtttaagcttcttcctccgattaagttttgtacatgtaaaacgacggccagt	1716
tgatgctttttgaagttttcatggcatgatttagcatttgaaatataatgagaaaagagccctttaacttacagaagtaaggaaacagctatgaccatg	1717

Acknowledgements

We would like to thank the imaging platform of Toulouse TRI for their assistance. This work was supported by the *Agence Nationale de la Recherche* (ANDY) and the IDEX of Toulouse University (Clemgene and Nudgene). We thank Margaux Cescato, Lilian Guillot and Jorge Perez-Fernandez for strain and plasmid constructions. YCp50-26 carrying *RPA49* was kindly provided by P. Thuriaux. We also thank Melanie Panarotto for the Miller spread analysis. This work benefited from exchanges with all unit members, including Anthony Henras, Frederic Beckouët, Lise Dauban, and Marta Kwapisz. We thank Stephanie Balor and Vanessa Soldan from the METI platform for the TEM acquisitions. CFT was supported by grants BFU2013-48374-P and BFU2017-87397-P of the Spanish Ministry of Economy and Competitiveness, and by the Ramón Areces Foundation.

Bibliography

Albert B, Léger-Silvestre I, Normand C, Ostermaier MK, Pérez-Fernández J, Panov KI, Zomerdijk JCBM, Schultz P & Gadal O (2011) RNA polymerase I-specific subunits promote polymerase clustering to enhance the rRNA gene transcription cycle. *J Cell Biol* **192:** 277–293

Beckouet F, Labarre-Mariotte S, Albert B, Imazawa Y, Werner M, Gadal O, Nogi Y & Thuriaux P (2008) Two RNA polymerase I subunits control the binding and release of Rrn3 during transcription. *Mol Cell Biol* **28:** 1596–1605

Beltrame M & Tollervey D (1992) Identification and functional analysis of two U3 binding sites on yeast pre-ribosomal RNA. *EMBO J* **11:** 1531–1542

Berger AB, Cabal GG, Fabre E, Duong T, Buc H, Nehrbass U, Olivo-Marin J-C, Gadal O & Zimmer C (2008) High-resolution statistical mapping reveals gene territories in live yeast. *Nat Methods* **5:** 1031–1037

Berger AB, Decourty L, Badis G, Nehrbass U, Jacquier A & Gadal O (2007) Hmo1 is required for TOR-dependent regulation of ribosomal protein gene transcription. *Mol Cell Biol* **27:** 8015–8026

Blattner C, Jennebach S, Herzog F, Mayer A, Cheung ACM, Witte G, Lorenzen K, Hopfner K-P, Heck AJR, Aebersold R & Cramer P (2011) Molecular basis of Rrn3-regulated RNA polymerase I initiation and cell growth. *Genes Dev* **25:** 2093–2105

Chambon P (1975) Eukaryotic nuclear RNA polymerases. *Annu Rev Biochem* **44:** 613–638

Chen H-T, Warfield L & Hahn S (2007) The positions of TFIIF and TFIIE in the RNA polymerase II transcription preinitiation complex. *Nat Struct Mol Biol* **14:** 696–703

Cioci F, Vu L, Eliason K, Oakes M, Siddiqi IN & Nomura M (2003) Silencing in yeast rDNA chromatin: reciprocal relationship in gene expression between RNA polymerase I and II. *Mol Cell* **12:** 135–145

Cramer P, Bushnell DA & Kornberg RD (2001) Structural basis of transcription: RNA polymerase II at 2.8 angstrom resolution. *Science* **292:** 1863–1876

Decourty L, Saveanu C, Zemam K, Hantraye F, Frachon E, Rousselle J-C, Fromont-Racine M & Jacquier A (2008) Linking functionally related genes by sensitive and quantitative characterization of genetic interaction profiles. *Proc Natl Acad Sci U S A* **105:** 5821–5826

Drygin D, Rice WG & Grummt I (2010) The RNA polymerase I transcription machinery: an emerging target for the treatment of cancer. *Annu Rev Pharmacol Toxicol* **50:** 131–156

Engel C, Gubbey T, Neyer S, Sainsbury S, Oberthuer C, Baejen C, Bernecky C & Cramer P (2017) Structural basis of RNA polymerase I transcription initiation. *Cell* **169:** 120–131.e22

Engel C, Plitzko J & Cramer P (2016) RNA polymerase I-Rrn3 complex at 4.8 Å resolution. *Nat Commun* **7:** 12129

Engel C, Sainsbury S, Cheung AC, Kostrewa D & Cramer P (2013) RNA polymerase I structure and transcription regulation. *Nature* **502:** 650–655

Fernández-Tornero C (2018) RNA polymerase I activation and hibernation: unique mechanisms for unique genes. *Transcription*: 1–7

Fernández-Tornero C, Moreno-Morcillo M, Rashid UJ, Taylor NMI, Ruiz FM, Gruene T, Legrand P, Steuerwald U & Müller CW (2013) Crystal structure of the 14-subunit

RNA polymerase I. *Nature* **502:** 644–649
Gadal O, Labarre S, Boschiero C & Thuriaux P (2002) Hmo1, an HMG-box protein, belongs to the yeast ribosomal DNA transcription system. *EMBO J* **21:** 5498–5507
Gadal O, Mariotte-Labarre S, Chedin S, Quemeneur E, Carles C, Sentenac A & Thuriaux P (1997) A34.5, a nonessential component of yeast RNA polymerase I, cooperates with subunit A14 and DNA topoisomerase I to produce a functional rRNA synthesis machine. *Mol Cell Biol* **17:** 1787–1795
Geiger SR, Lorenzen K, Schreieck A, Hanecker P, Kostrewa D, Heck AJR & Cramer P (2010) RNA polymerase I contains a TFIIF-related DNA-binding subcomplex. *Mol Cell* **39:** 583–594
Ghaemmaghami S, Huh W-K, Bower K, Howson RW, Belle A, Dephoure N, O'Shea EK & Weissman JS (2003) Global analysis of protein expression in yeast. *Nature* **425:** 737–741
Ghavi-Helm Y, Michaut M, Acker J, Aude J-C, Thuriaux P, Werner M & Soutourina J (2008) Genome-wide location analysis reveals a role of TFIIS in RNA polymerase III transcription. *Genes Dev* **22:** 1934–1947
Han Y, Yan C, Nguyen THD, Jackobel AJ, Ivanov I, Knutson BA & He Y (2017) Structural mechanism of ATP-independent transcription initiation by RNA polymerase I. *elife* **6:**
Hermann-Le Denmat S, Werner M, Sentenac A & Thuriaux P (1994) Suppression of yeast RNA polymerase III mutations by FHL1, a gene coding for a fork head protein involved in rRNA processing. *Mol Cell Biol* **14:** 2905–2913
Hoffmann NA, Jakobi AJ, Moreno-Morcillo M, Glatt S, Kosinski J, Hagen WJH, Sachse C & Müller CW (2015) Molecular structures of unbound and transcribing RNA polymerase III. *Nature* **528:** 231–236
Huet J, Buhler JM, Sentenac A & Fromageot P (1975) Dissociation of two polypeptide chains from yeast RNA polymerase A. *Proc Natl Acad Sci U S A* **72:** 3034–3038
Hull MW, McKune K & Woychik NA (1995) RNA polymerase II subunit RPB9 is required for accurate start site selection. *Genes Dev* **9:** 481–490
Keener J, Josaitis CA, Dodd JA & Nomura M (1998) Reconstitution of yeast RNA polymerase I transcription in vitro from purified components. TATA-binding protein is not required for basal transcription. *J Biol Chem* **273:** 33795–33802
Kuhn C-D, Geiger SR, Baumli S, Gartmann M, Gerber J, Jennebach S, Mielke T, Tschochner H, Beckmann R & Cramer P (2007) Functional architecture of RNA polymerase I. *Cell* **131:** 1260–1272
Landrieux E, Alic N, Ducrot C, Acker J, Riva M & Carles C (2006) A subcomplex of RNA polymerase III subunits involved in transcription termination and reinitiation. *EMBO J* **25:** 118–128
Liljelund P, Mariotte S, Buhler JM & Sentenac A (1992) Characterization and mutagenesis of the gene encoding the A49 subunit of RNA polymerase A in Saccharomyces cerevisiae. *Proc Natl Acad Sci U S A* **89:** 9302–9305
Longtine MS, Mckenzie III A, Demarini DJ, Shah NG, Wach A, Brachat A, Philippsen P & Pringle JR (1998) Additional modules for versatile and economical PCR-based gene deletion and modification in Saccharomyces cerevisiae. *Yeast*
Merkl P, Perez-Fernandez J, Pilsl M, Reiter A, Williams L, Gerber J, Böhm M, Deutzmann R, Griesenbeck J, Milkereit P & Tschochner H (2014) Binding of the termination factor Nsi1 to its cognate DNA site is sufficient to terminate RNA polymerase I transcription in vitro and to induce termination in vivo. *Mol Cell Biol* **34:** 3817–3827

Miller OL & Beatty BR (1969) Visualization of nucleolar genes. *Science* **164:** 955–7
Van Mullem V, Landrieux E, Vandenhaute J & Thuriaux P (2002) Rpa12p, a conserved RNA polymerase I subunit with two functional domains. *Mol Microbiol* **43:** 1105–1113
Neyer S, Kunz M, Geiss C, Hantsche M, Hodirnau V-V, Seybert A, Engel C, Scheffer MP, Cramer P & Frangakis AS (2016) Structure of RNA polymerase I transcribing ribosomal DNA genes. *Nature* **540:** 607–610
Nogi Y, Yano R, Dodd J, Carles C & Nomura M (1993) Gene RRN4 in Saccharomyces cerevisiae encodes the A12.2 subunit of RNA polymerase I and is essential only at high temperatures. *Mol Cell Biol* **13:** 114–122
Osheim YN, French SL, Sikes ML & Beyer AL (2009) Electron microscope visualization of RNA transcription and processing in Saccharomyces cerevisiae by Miller chromatin spreading. *Methods Mol Biol* **464:** 55–69
Peyroche G, Milkereit P, Bischler N, Tschochner H, Schultz P, Sentenac A, Carles C & Riva M (2000) The recruitment of RNA polymerase I on rDNA is mediated by the interaction of the A43 subunit with Rrn3. *EMBO J* **19:** 5473–5482
Pilsl M, Crucifix C, Papai G, Krupp F, Steinbauer R, Griesenbeck J, Milkereit P, Tschochner H & Schultz P (2016) Structure of the initiation-competent RNA polymerase I and its implication for transcription. *Nat Commun* **7:** 12126
Prescott EM, Osheim YN, Jones HS, Alen CM, Roan JG, Reeder RH, Beyer AL & Proudfoot NJ (2004) Transcriptional termination by RNA polymerase I requires the small subunit Rpa12p. *Proc Natl Acad Sci U S A* **101:** 6068–6073
Sadian Y, Tafur L, Kosinski J, Jakobi AJ, Wetzel R, Buczak K, Hagen WJ, Beck M, Sachse C & Müller CW (2017) Structural insights into transcription initiation by yeast RNA polymerase I. *EMBO J* **36:** 2698–2709
Sambrook J, Fritsch EF & Maniatis T (1989) Molecular cloning: a laboratory manual. *Molecular cloning: a laboratory manual.* Available at: https://www.cabdirect.org/cabdirect/abstract/19901616061
Schiestl RH & Gietz RD (1989) High efficiency transformation of intact yeast cells using single stranded nucleic acids as a carrier. *Curr Genet* **16:** 339–346
Sherman F, Fink GR & Hicks JBN (1986) Methods in Yeast Genetics. A Laboratory Course Manual. New York: Cold Spring Harbor Laboratory
Sikorski RS & Hieter P (1989) A system of shuttle vectors and yeast host strains designed for efficient manipulation of DNA in Saccharomyces cerevisiae. *Genetics* **122:** 19–27
Sung M-K, Ha CW & Huh W-K (2008) A vector system for efficient and economical switching of C-terminal epitope tags in Saccharomyces cerevisiae. *Yeast* **25:** 301–311
Tafur L, Sadian Y, Hoffmann NA, Jakobi AJ, Wetzel R, Hagen WJH, Sachse C & Müller CW (2016) Molecular structures of transcribing RNA polymerase I. *Mol Cell* **64:** 1135–1143
Torreira E, Louro JA, Pazos I, González-Polo N, Gil-Carton D, Duran AG, Tosi S, Gallego O, Calvo O & Fernández-Tornero C (2017) The dynamic assembly of distinct RNA polymerase I complexes modulates rDNA transcription. *elife* **6:**
Tschochner H (1996) A novel RNA polymerase I-dependent RNase activity that shortens nascent transcripts from the 3' end. *Proc Natl Acad Sci U S A* **93:** 12914–12919
Viktorovskaya OV, Appling FD & Schneider DA (2011) Yeast transcription elongation factor Spt5 associates with RNA polymerase I and RNA polymerase II directly. *J Biol Chem* **286:** 18825–18833

Walmacq C, Kireeva ML, Irvin J, Nedialkov Y, Lubkowska L, Malagon F, Strathern JN & Kashlev M (2009) Rpb9 subunit controls transcription fidelity by delaying NTP sequestration in RNA polymerase II. *J Biol Chem* **284:** 19601–19612

Warner JR (1999) The economics of ribosome biosynthesis in yeast. *Trends Biochem Sci* **24:** 437–440

Werner F (2008) Structural evolution of multisubunit RNA polymerases. *Trends Microbiol* **16:** 247–250

Wu C-C, Lin Y-C & Chen H-T (2011) The TFIIF-like Rpc37/53 dimer lies at the center of a protein network to connect TFIIIC, Bdp1, and the RNA polymerase III active center. *Mol Cell Biol* **31:** 2715–2728

Yamamoto RT, Nogi Y, Dodd JA & Nomura M (1996) RRN3 gene of Saccharomyces cerevisiae encodes an essential RNA polymerase I transcription factor which interacts with the polymerase independently of DNA template. *EMBO J* **15:** 3964–3973

Yano R, Oakes M, Yamaghishi M, Dodd JA & Nomura M (1992) Cloning and characterization of SRP1, a suppressor of temperature- sensitive RNA polymerase I mutations, in. *Mol Cell Biol* **12:** 5640–51

A

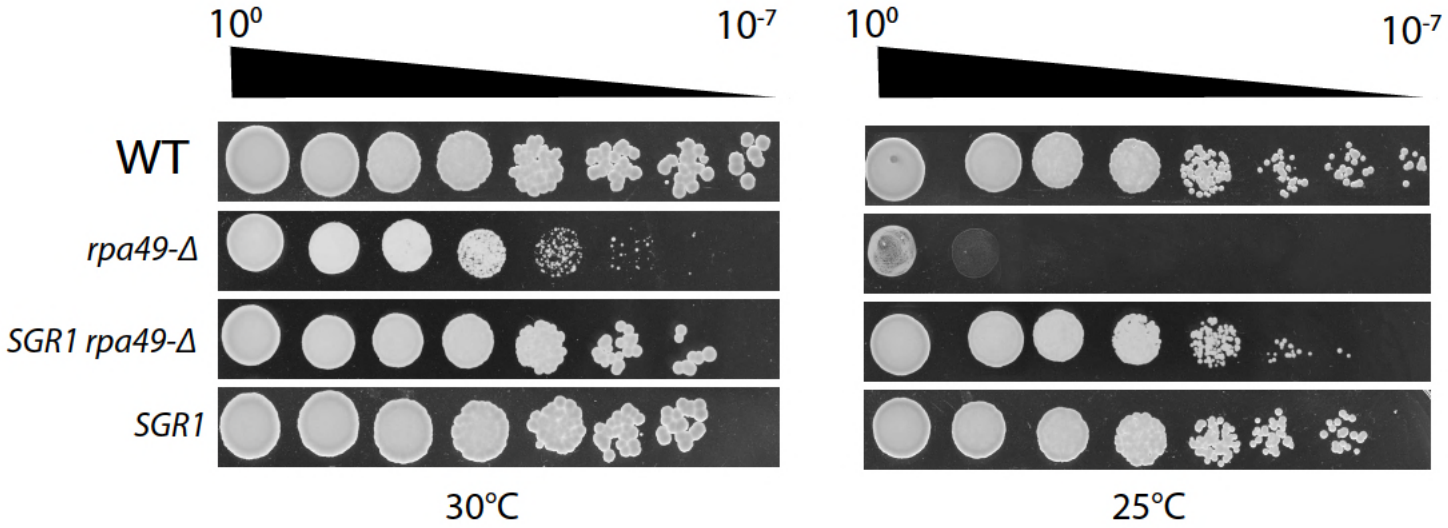
10⁰
10⁻⁷
10⁰
10⁻⁷
WT
rpa49-Δ
SGR1 rpa49-Δ
SGR1
30°C
25°C

B

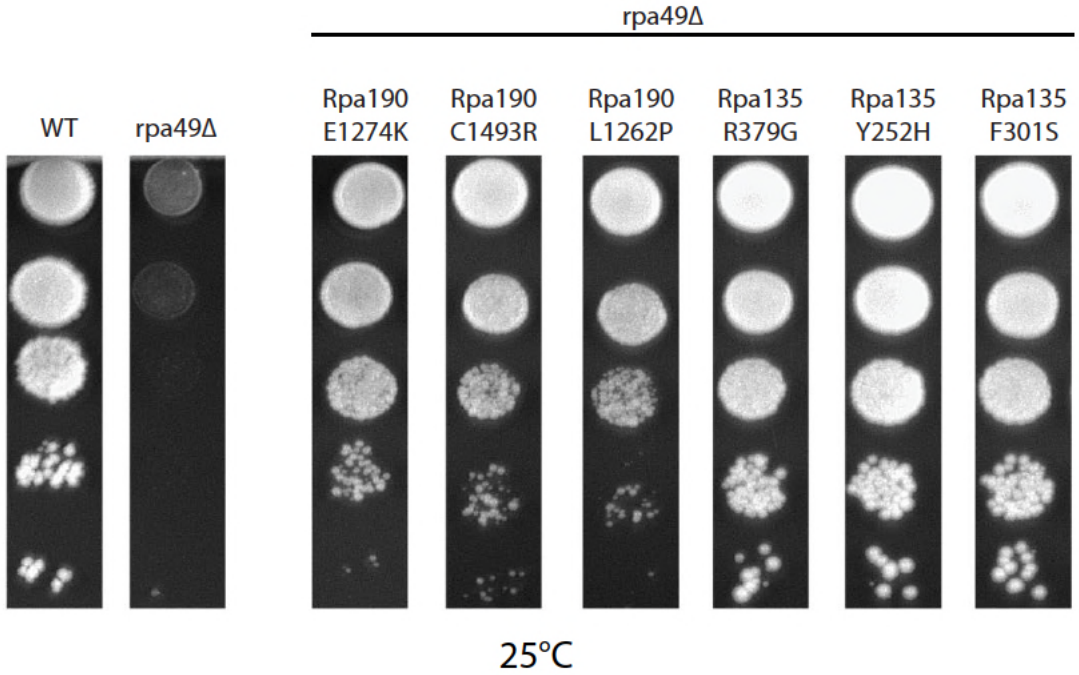
rpa49Δ
WT
rpa49Δ
Rpa190 E1274K
Rpa190 C1493R
Rpa190 L1262P
Rpa135 R379G
Rpa135 Y252H
Rpa135 F301S
25°C

Figure 1

A.

	Doubling time (min)
WT	104 +/- 2
Rpa49ΔC	292 +/- 11
RPA135-F301S	98 +/- 2
Rpa49ΔC RPA135-F301S	118 +/-3

B.

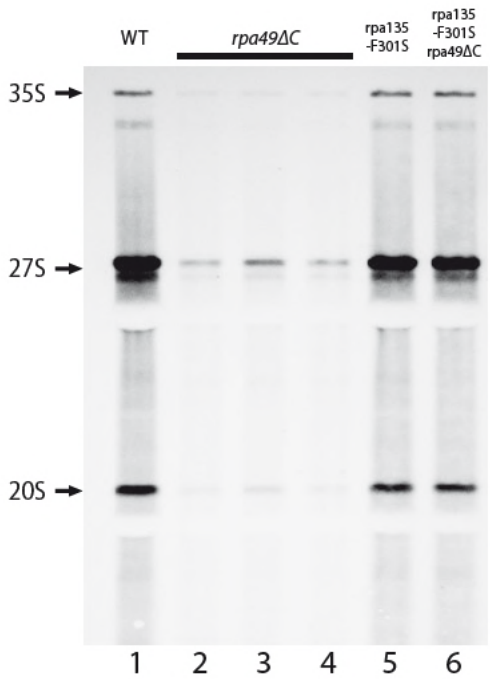

C.

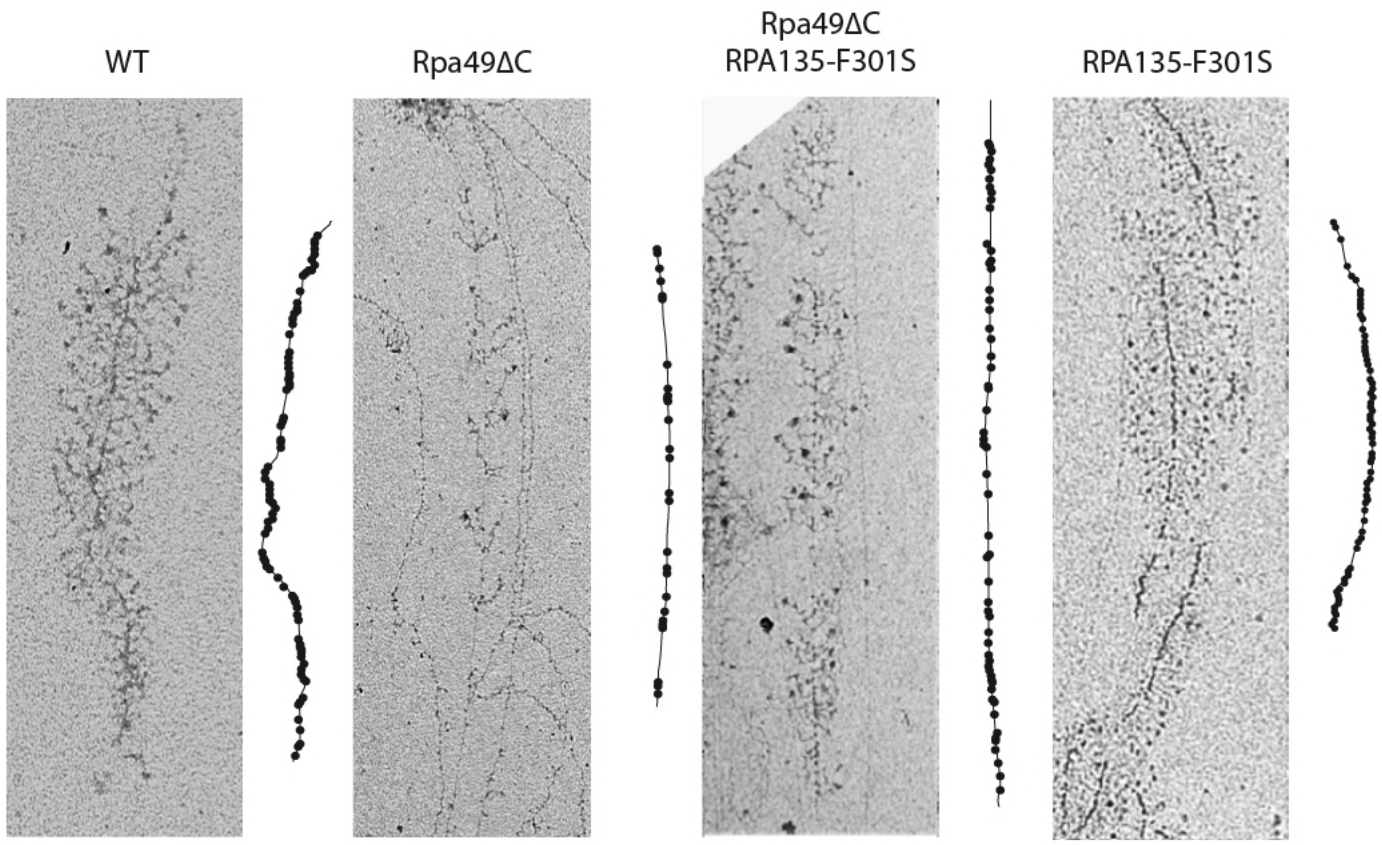

91 +/- 13
N=42

21 +/- 5
N=31

46 +/- 10
N=61

93 +/- 17
N=36

Figure 2.

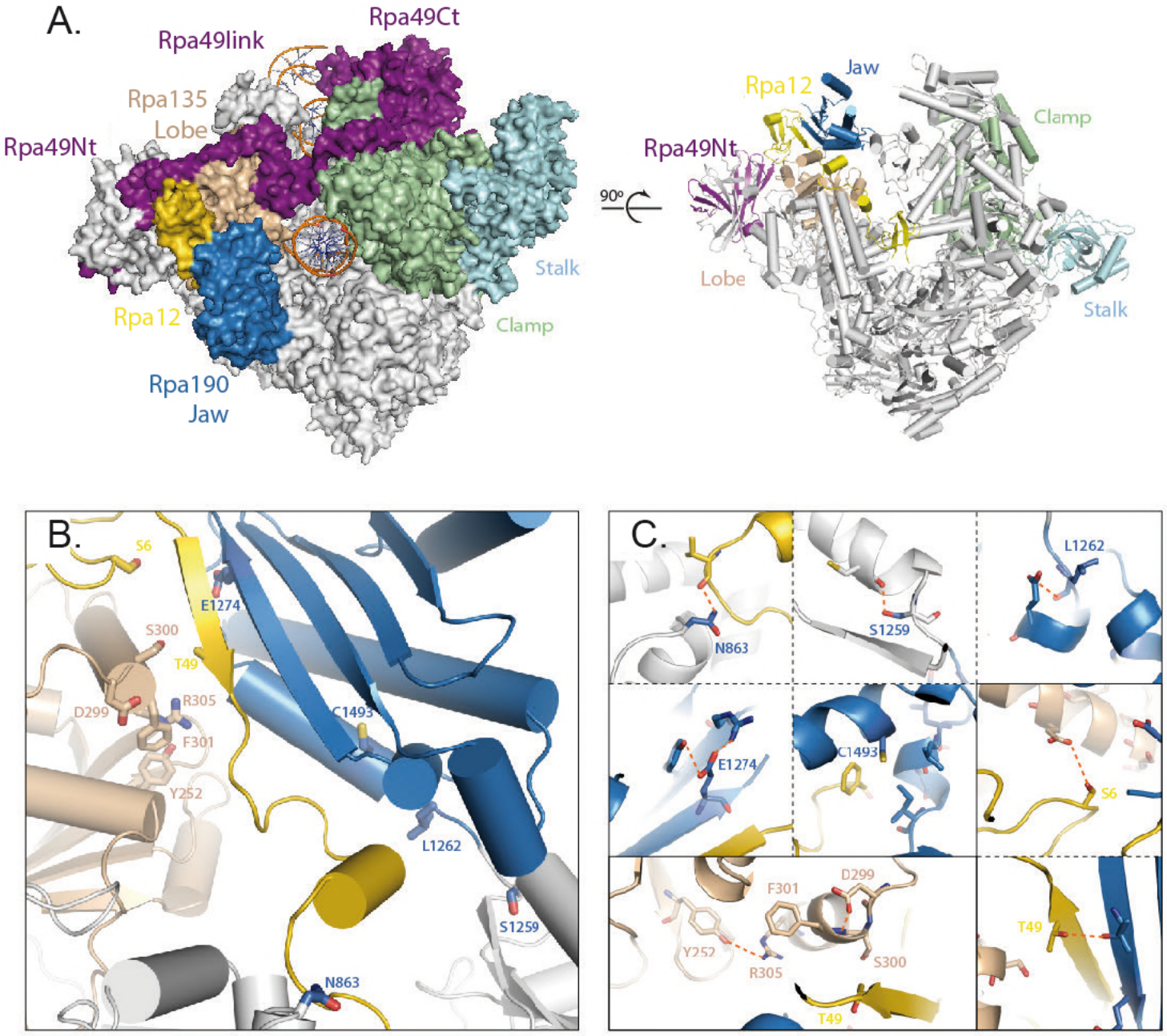
A.
Rpa49Ct
Rpa49link
Rpa135
Lobe
Rpa49Nt
Rpa12
Rpa190
Jaw
Stalk
Clamp
Jaw
Rpa12
Clamp
Rpa49Nt
90°
Lobe
Stalk
B.
S6
E1274
S300
T49
R305
D299
F301
Y252
C1493
L1262
S1259
N863
C.
N863
S1259
L1262
E1274
C1493
S6
F301
D299
Y252
R305
S300
T49
T49

Figure 3.

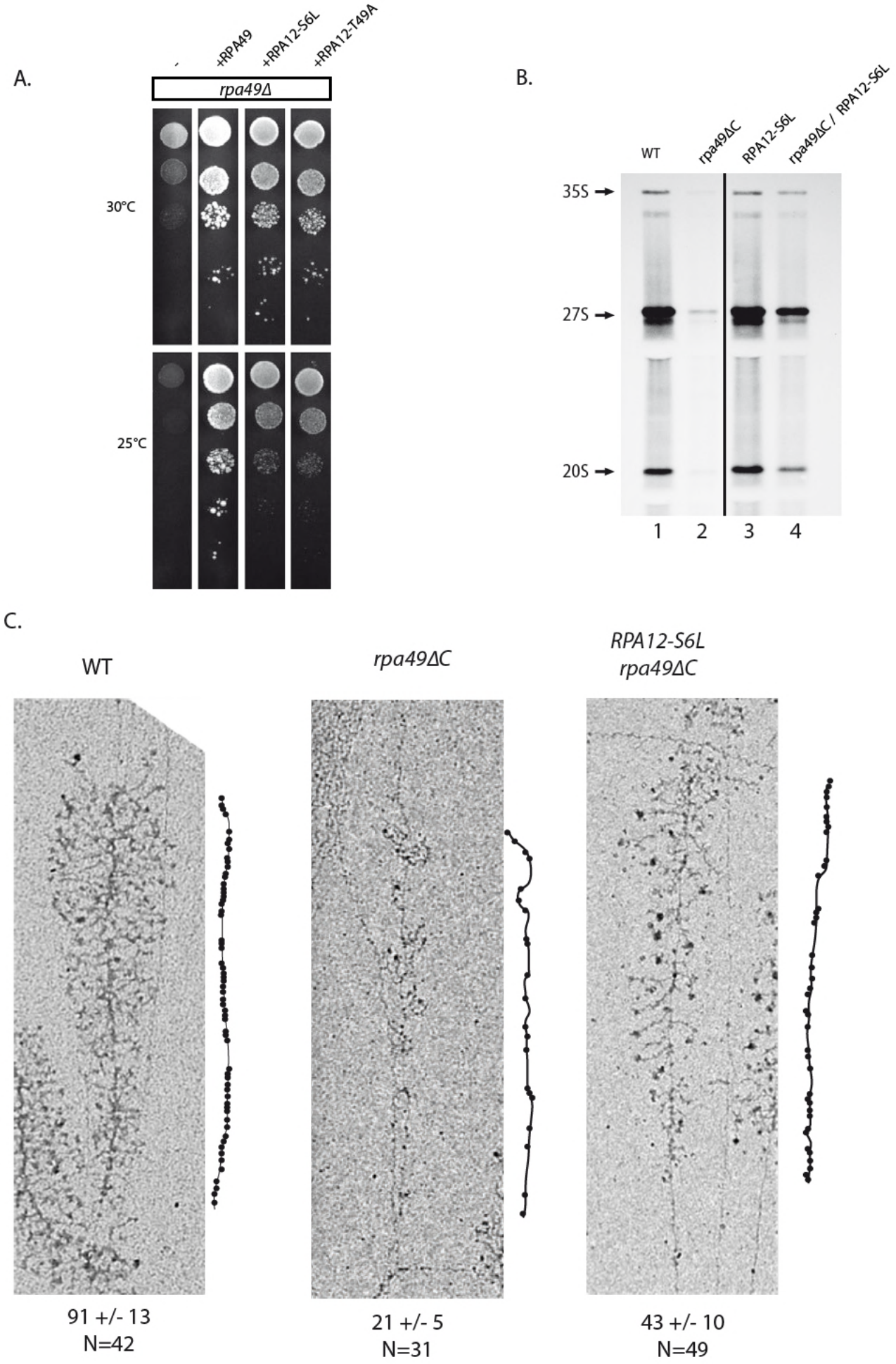
A.
-
+RPA49
+RPA12-S6L
+RPA12-T49A
rpa49Δ
30°C
25°C
B.
WT
rpa49ΔC
RPA12-S6L
rpa49ΔC / RPA12-S6L
35S
27S
20S
1
2
3
4
C.
WT
rpa49ΔC
RPA12-S6L
rpa49ΔC
91 +/- 13
N=42
21 +/- 5
N=31
43 +/- 10
N=49

Figure 4.

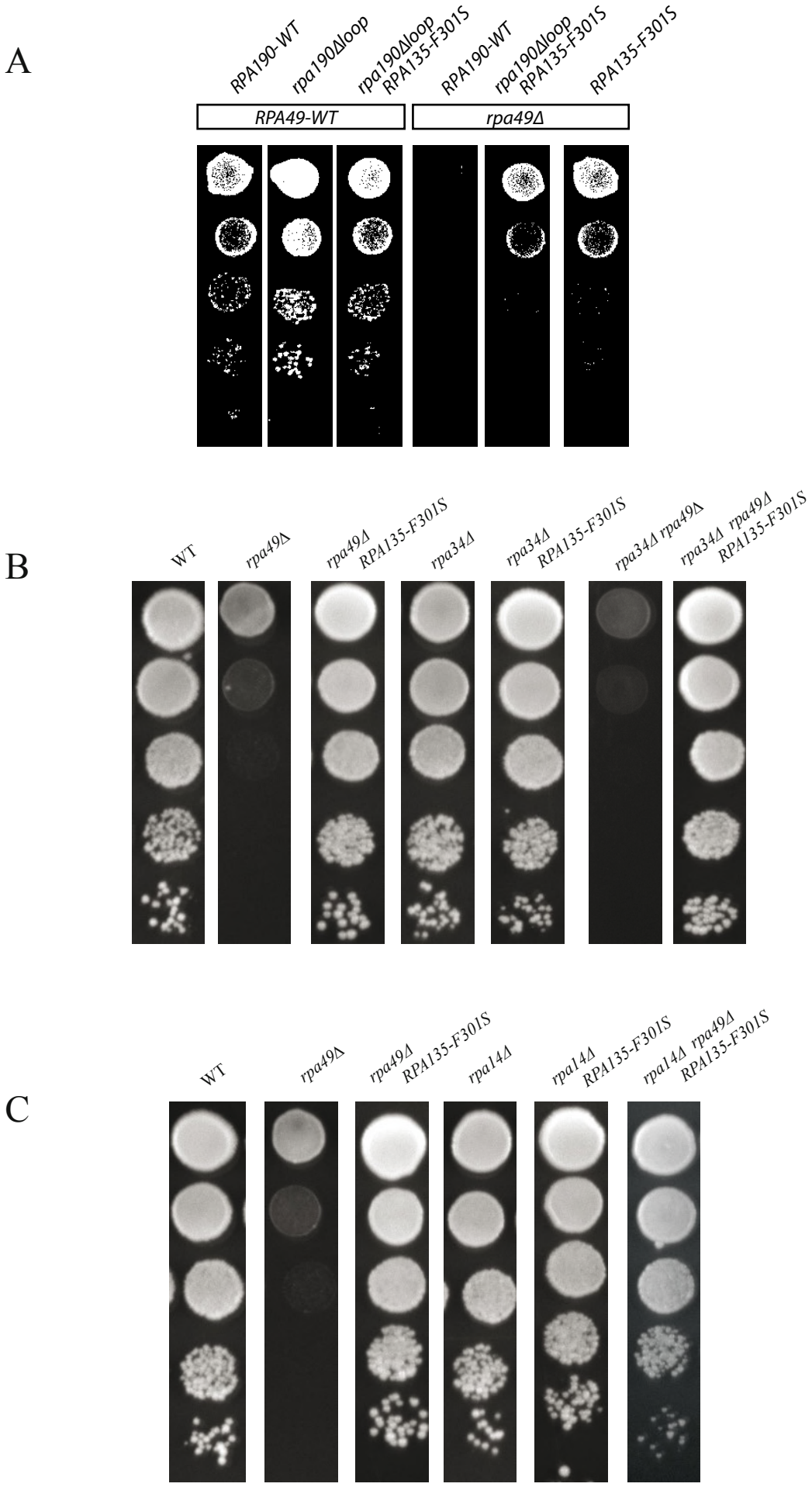
A
RPA190-WT
rpa190Δloop
rpa190Δloop RPA135-F301S
RPA190-WT
rpa190Δloop RPA135-F301S
RPA135-F301S
RPA49-WT
rpa49Δ
B
WT
rpa49Δ
rpa49Δ RPA135-F301S
rpa34Δ
rpa34Δ RPA135-F301S
rpa34Δ rpa49Δ
rpa34Δ rpa49Δ RPA135-F301S
C
WT
rpa49Δ
rpa49Δ RPA135-F301S
rpa14Δ
rpa14Δ RPA135-F301S
rpa14Δ rpa49Δ RPA135-F301S

Figure 5.

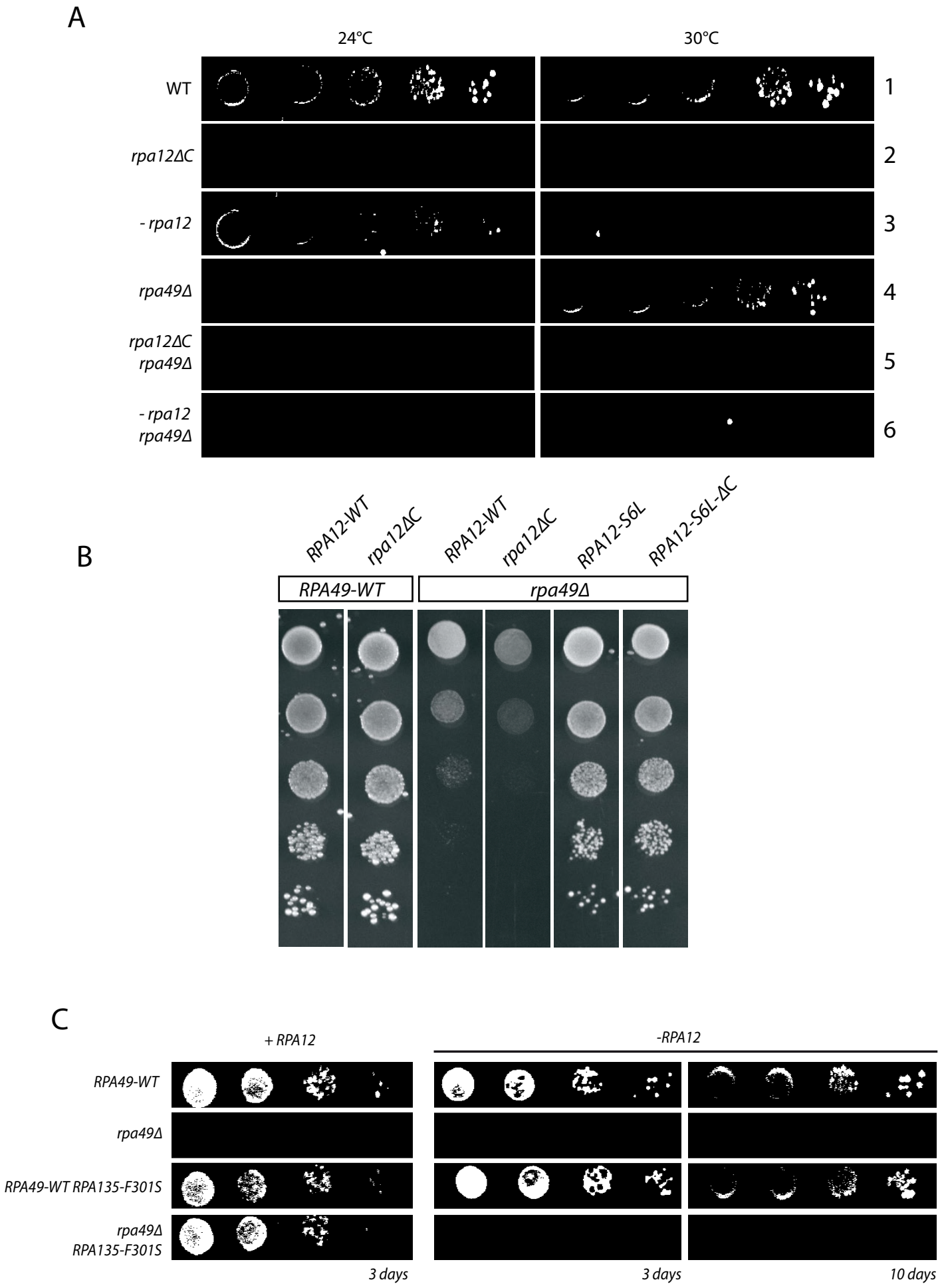
A
24°C
30°C
WT
rpa12ΔC
- rpa12
rpa49Δ
rpa12ΔC
rpa49Δ
- rpa12
rpa49Δ
1
2
3
4
5
6
B
RPA12-WT
rpa12ΔC
RPA12-WT
rpa12ΔC
RPA12-S6L
RPA12-S6L-ΔC
RPA49-WT
rpa49Δ
C
+ RPA12
-RPA12
RPA49-WT
rpa49Δ
RPA49-WT RPA135-F301S
rpa49Δ
RPA135-F301S
3 days
3 days
10 days

Figure 6.

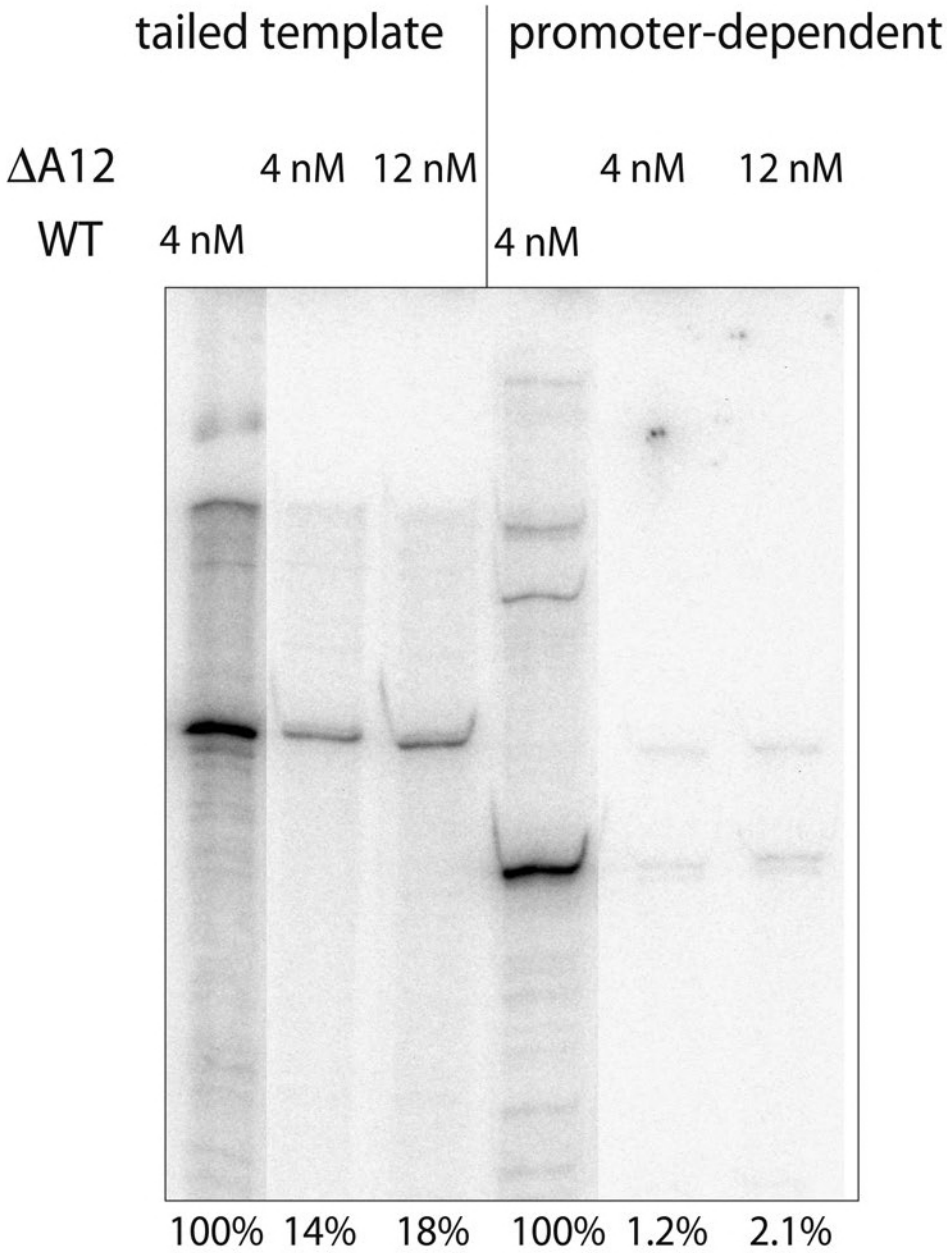
tailed template
promoter-dependent
ΔA12
4 nM
12 nM
4 nM
12 nM
WT
4 nM
4 nM
100%
14%
18%
100%
1.2%
2.1%

Figure 7.

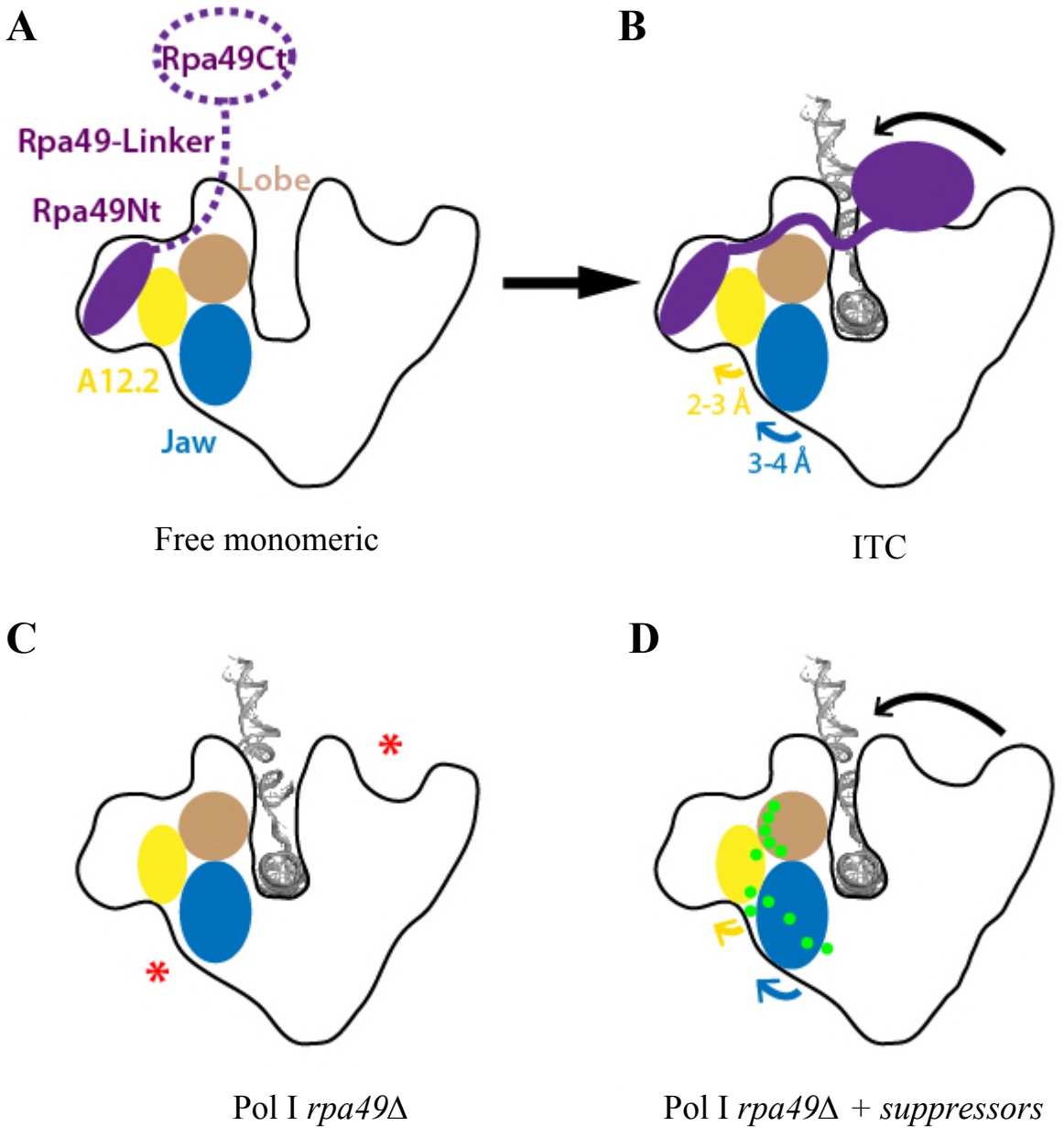
A
Rpa49Ct
Rpa49-Linker
Lobe
Rpa49Nt
A12.2
Jaw
Free monomeric
B
2-3 Å
3-4 Å
ITC
C
Pol I rpa49Δ
D
Pol I rpa49Δ + suppressors

Figure 8

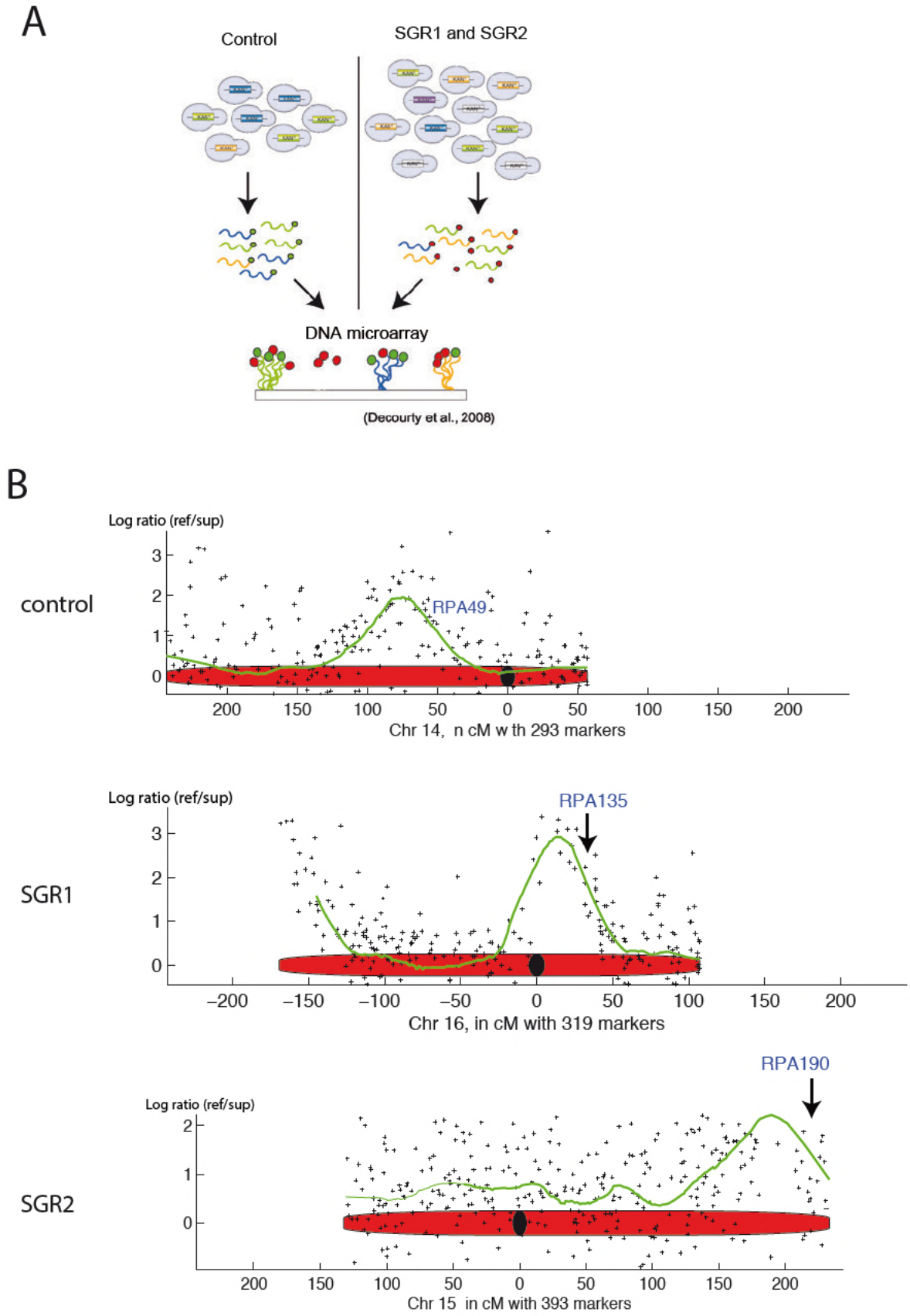

Suppl. Figure 1 : Genetic interaction mapping (GIM) to identify suppressor mutations in SGR1 and SGR2. (A) Schematic representation of GIM interaction assay. Enrichment ratio between control and SGR are used as read-out to map genetic interactions. (B) Relative enrichment of each barcode (black cross) along chromosome (in red) are used to map genetic linkage. Green curve represents mean in a sliding windows of 20 barcodes. Local maximum in such curve was used to identify locus of interest: *RPA49* as positive control (upper panel, chr 14); *RPA135* in SGR1 (middle panel, chr 16) ; *RPA190* in SGR2 (lower panel, chr 15).